

## Seasonal Variability of Bio-Optical and Physical Properties in the Sargasso Sea

T. DICKEY,<sup>1</sup> T. GRANATA,<sup>1</sup> J. MARRA,<sup>2</sup> C. LANGDON,<sup>2</sup> J. WIGGERT,<sup>1</sup>  
 Z. CHAI-JOCHNER,<sup>1</sup> M. HAMILTON,<sup>1,3</sup> J. VAZQUEZ,<sup>3</sup> M. STRAMSKA,<sup>1</sup>  
 R. BIDIGARE,<sup>4</sup> AND D. SIEGEL<sup>1,5</sup>

The seasonal variability of bio-optical and physical properties within the upper ocean at a site in the Sargasso Sea (34°N, 70°W) has been observed using multivariable moored systems (MVMS) during a 9-month period (March through November 1987). In addition, complementary meteorological data, sea surface height (Geosat) and sea surface temperature maps, and expendable bathythermograph (XBT) and shipboard profile data (physical and bio-optical) have been utilized for interpretation. The observations during March are characteristic of late wintertime conditions of a deep isothermal layer (~18-19°C), but with intervening periods of warming due to the advection of warm outbreak waters associated with Gulf Stream meanders. The mixed layer depth shoals from greater than 160 m to about 25 m in late March (spring transition). Phytoplankton blooms follow the mixed layer shoaling. A succession of phytoplankton populations occurs during this transitional interval. Mesoscale variability associated with cold core rings and warm outbreak waters associated with the Gulf Stream are evident at various times. The mixed layer remains near 25 m for the summer and deepens in mid-September. A relatively intense subsurface maximum in chlorophyll develops at ~75 m following the spring transition. The maximum persists, but weakens in mid-summer. The present study clearly indicates that important processes associated with and contributing to the seasonal cycle occur on short time and space scales and that integrated data sets obtained from moorings, ships, and satellites can be used to effectively study bio-optical and physical phenomena on time scales from minutes to seasons.

### 1. INTRODUCTION

The present study, a major component of the Office of Naval Research sponsored Biowatt program (Biowatt I conducted in 1985 and Biowatt II conducted in 1987), concerns the ecology of the upper ocean planktonic community and was motivated in part by the desire to improve our understanding of the variability of upper ocean bio-optical properties as affected by physical forcing. The present measurements enable the determination of cyclic (e.g., diurnal, tidal, seasonal) and episodic (e.g., synoptic weather event scale, advective transport of materials, phytoplankton blooms) changes in the physical, optical, and biological environment [Dickey *et al.*, 1986, 1991; Smith *et al.*, 1991; Marra *et al.*, 1992].

The biological, as well as physical, dynamics of the pelagic ocean are highly intermittent; yet time series observations relevant to bio-optical processes and primary productivity have been either coarse in temporal resolution (e.g., bi-weekly), short in duration (e.g., typically a maximum of a few weeks), or done in coastal waters or lakes [see Dickey, 1991; Dickey *et al.*, 1991; Smith *et al.*, 1991]. The observations reported here and those presented earlier in Dickey *et al.* [1991] and Smith *et al.* [1991] and in a recent companion paper by Marra *et al.* [1992] are the first long-term, high-resolution time series measurements of bio-optical and physical variables in the open ocean.

Our data may be used to identify critical processes and feedback mechanisms, statistically quantify relationships, and formulate and test coupled bio-optical and physical models. Data obtained from the instrument platform, the multivariable moored system (MVMS), may also be used for estimating biomass from beam attenuation and chlorophyll fluorescence (strobe-stimulated) measurements, for primary productivity determinations using beam attenuation, dissolved oxygen, stimulated chlorophyll fluorescence, and photosynthetically available radiation (PAR) data, and for estimating the vertical flux of particulate carbon from the euphotic layer [e.g., Dickey, 1991]. Estimates of pigment biomass and primary productivity using data obtained from the MVMS can be intercompared and used for examining variations in the attenuation of solar radiation due to distributions of pigment concentration [e.g., Siegel and Dickey, 1987]. Determining and modeling primary productivity and carbon flux are of considerable interest in the context of global biogeochemical fluxes across the air-sea interface and through the interior of the ocean as they relate to the global carbon budget [e.g., Brewer *et al.*, 1986]. Moored systems utilized for the present work can be used to provide relevant bio-optical and physical information on time scales unachievable from sampling by ship, airplane, or satellite platforms and depth scales inaccessible from the latter two platform types. The utilization of all of these platforms will be necessary for global monitoring and modeling of the upper ocean's ecology and the flux of carbon from the upper ocean [e.g., Dickey, 1991].

The present report focuses on (1) local physical forcing at the mooring site, (2) mesoscale features in the region of the mooring site, and (3) the seasonal evolution and variation of physical and bio-optical variables in the Sargasso Sea. Earlier relevant papers have focused on the spring transition in physical and bio-optical variables [Dickey *et al.*, 1990a,b, 1991], diurnal cycles of bio-optical properties [Hamilton *et al.*, 1990], short time scale variations in bio-optical properties caused by changing cloud cover [Stramska and Dickey, 1992a] and the evolution of optical properties and pigment biomass at the site [Smith *et al.*, 1991]. A recent companion paper by

<sup>1</sup> Ocean Physics Group, Department of Geological Sciences, University of Southern California, Los Angeles.

<sup>2</sup> Lamont-Doherty Geological Observatory of Columbia University, Palisades, New York.

<sup>3</sup> Jet Propulsion Laboratory, Pasadena, California.

<sup>4</sup> Department of Oceanography, University of Hawaii, Honolulu.

<sup>5</sup> Center for Remote Sensing and Environmental Optics, University of California, Santa Barbara.

Copyright 1993 by the American Geophysical Union.

Paper number 92JC01830.

0148-0227/93/92JC-01830\$05.00

## BIOWATT STUDY REGION

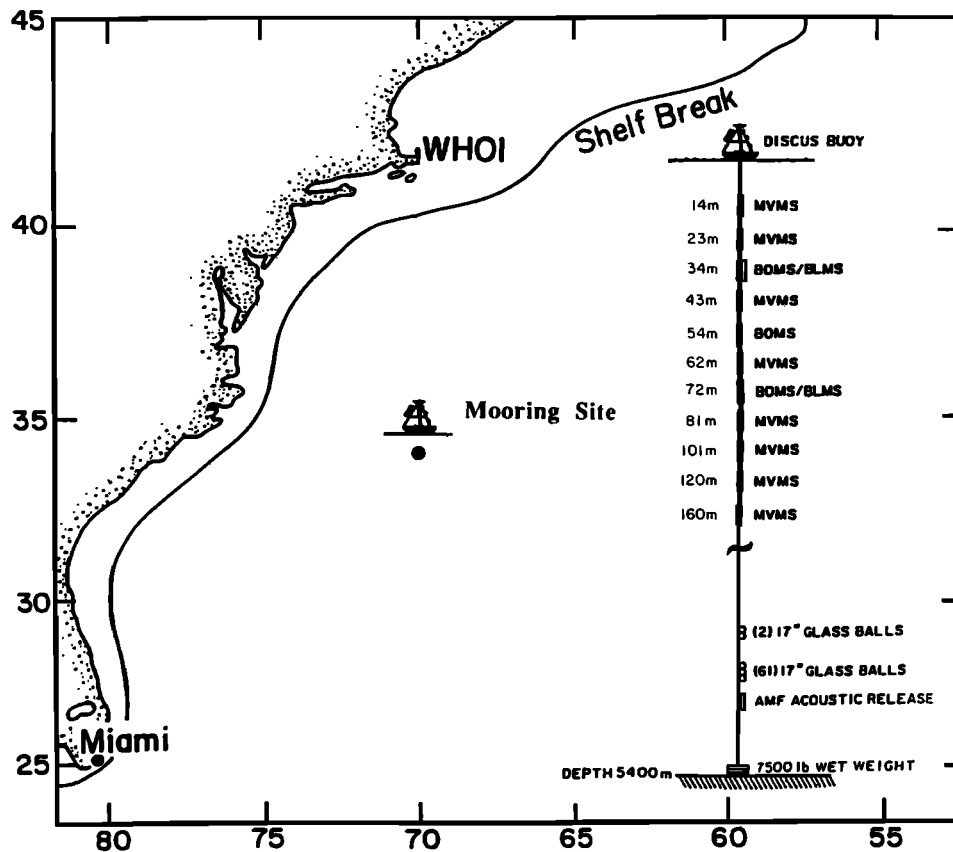


Fig. 1. Location of the Biowatt II mooring for the 1987 field study in the Sargasso Sea and the Biowatt II mooring configuration including the depths of the MVMS, BOMS, and BLMS systems.

Marra *et al.* [1992] focuses on an optical determination of the seasonal signal of primary production at the site. The results presented here and in Marra *et al.* [1992] may be used for comparison with other observational studies and to develop and test interdisciplinary models of the seasonal cycle with high temporal resolution data. In addition, ecological questions concerning the role of episodic forcing, mesoscale structures (e.g., advection), and the need for high sampling rates (e.g., aliasing problem) may be addressed.

## 2. METHODS

The site of the Biowatt II mooring was in the open ocean waters (depth ~5400 m) of the Sargasso Sea (34°N, 70°W; Figure 1). Individual moorings were deployed at the site in 1987 during three periods (February 28 to May 11, May 13 to August 30, and August 31 to November 23, see Table 1). The observations considered here focus on moored measurements taken with the MVMS, meteorological sensors mounted on the surface buoy of the mooring, surface temperature maps, and sea surface height (SSH) data obtained from Geosat. In addition, other complementary data sets described below are used to interpret the evolution of the physical and bio-optical variables in the region of the mooring.

The sensor suite for the MVMS includes: a vector measuring current meter (VMCM) for horizontal velocity measurements [Weller and Davis, 1980], a thermistor for temperature measurements, a conductivity sensor (on 14 m and 160 m MVMS's only), a beam transmissometer [Bartz *et al.*, 1978], a strobe in situ fluorometer [Bartz *et al.*, 1988], a PAR sensor

TABLE 1. Deployment Periods and Dates.

Deployment	Period	Julian Day
1	1	60-79
	2	79-86
	3	86-102
	4	102-106
	5	106-119
	6	119-130
2	7	136-156
	8	156-180
	9	180-195
	10	195-210
	11	210-220
	12	220-242
3	13	243-250
	14	250-263
	15	263-275
	16	275-300
	17	300-314
	18	314-327

[Booth, 1976], and a pulsed electrode dissolved oxygen sensor [Langdon, 1984]. Antifoulants were applied to various components of the system. Our results suggest that the antifoulants were effective with minimal degradation of data because of biofouling effects. Predeployment calibrations were done for most sensors, however, postdeployment calibrations were not always possible. Shipboard profile measurements

done near the mooring site were used to intercompare with mooring measurements. These were useful, but direct comparisons were treated with caution because of spatial variability. Details concerning the MVMS may be found in *Dickey et al.* [1991].

Data were taken every 4 min and consisted of 4-min averages for all sensors except the fluorometer and the dissolved oxygen sensor, which were sampled instantaneously. Laboratory calibrations were done for thermistors and conductivity sensors, although the conductivity measurements were not useful for the interpretation of the data because of the limited dynamic range settings of the sensors. The beam transmissometers were calibrated in air free of obstruction and with the light path blocked before and after each deployment.

The beam attenuation coefficient is the sum of both absorption and scattering coefficients and is considered an inherent optical property. The value of the beam attenuation coefficient at 660 nm can be affected by variations of particle (in the open ocean, primarily phytoplankton or their products) concentrations, size distributions, shape, and refractive index [e.g., *Baker and Lavelle*, 1984; *Morel and Bricaud*, 1986]. One of the applications of this measurement is for particle concentration as the beam attenuation coefficient at 660 nm has been shown to correlate well with suspended particle concentrations, principally because of particle scattering [e.g., *Bishop*, 1986; *Spinrad et al.*, 1989]. It is important to keep in mind that phytoplankton physiological processes can act to modify the beam attenuation coefficient ( $c_{660}$ ). A possible mechanism causing  $c_{660}$  variations involves phytoplankton cell swelling accompanied by changes of cell size and refractive index [*Ackleson et al.*, 1990]. In situ diel changes in phytoplankton cell size have been suggested to be the cause of diel patterns in forward-angle light scatter [*Olson et al.*, 1990]. It should be noted that beam attenuation coefficient has been shown to respond to changes in light intensity on time scales considerably shorter than a day [*Stramska and Dickey*, 1992a,b].

The fluorometers were calibrated in the laboratory prior to (and after; prior data only were used here) each cruise using a phytoplankton culture of *Thalassiosira pseudonana*, a centric diatom, and the fluorescence signal was well-correlated with chlorophyll *a*. The various errors associated with this measurement were estimated to total between 10 and 20% [*Marra et al.*, 1992]. The interpretation of chlorophyll fluorescence is quite complex [e.g., *Falkowski and Kiefer*, 1985; review by *Prezelin et al.*, 1991]. For example, changes in chlorophyll fluorescence can be produced by variations in chlorophyll concentration and/or the fluorescence yield per chlorophyll concentration (i.e., the FI/Chl ratio). Changes in the FI/Chl ratio can be caused by variations in growth irradiance, quantum efficiency, the degree of chloroplast self-shading, and the photoadaptive state of the resident phytoplankton [e.g., *Falkowski*, 1980, 1984; *Kiefer et al.*, 1989]. Phytoplankton can change their cellular concentrations [*Falkowski*, 1980] and thus changes in chlorophyll may not always reflect changes in plant biomass.

PAR sensors measured quantum scalar irradiance in the waveband 400 - 700 nm. The PAR sensors and current meters were calibrated by the manufacturers. The PAR data were used to derive two useful quantities: PAR/PAR(0) or the ratio PAR at a given depth to surface PAR (actually just below sea surface) and KPAR which is the diffuse attenuation coefficient of PAR or

$$KPAR(z) = -(1/\Delta z) \ln[PAR(z+\Delta z)/PAR(z)]$$

There are limitations with the strict interpretation of KPAR because of the well-known differential spectral attenuation of light with depth. However, the spectral diffuse attenuation coefficient time series as well as the modeled chlorophyll *a* time

series computed for the bio-optical moored systems (BOMS) data (described below) by *Smith et al.* [1991] are qualitatively consistent with our KPAR and stimulated fluorescence time series. Another light parameter, the low light level (LLL) is defined here as a value of PAR below which net phytoplankton growth rate (community) is zero in the presence of naturally occurring losses (based on arguments by *Nelson and Smith* [1991]; also M. J. Perry and J. Marra, unpublished data, 1991). Values of LLL are species dependent (e.g., by at least a factor of 30 [*Langdon*, 1987, 1988]) and thus interpretation of depths of the LLL depth needs to be done with caution. For the present work, we have chosen a value of LLL of  $2.1 \times 10^{19}$  quanta  $m^{-2} s^{-1}$ , or approximately  $35 \mu E m^{-2} s^{-1}$  based on the work of M. J. Perry and J. Marra (unpublished data, 1991) as suggested by *Nelson and Smith* [1991]. The LLL is used as an aid in interpretation as it indicates photon flux available to phytoplankton opposed to the 1% light level where irradiance is normalized to a surface value. Hence, the effects of clouds are included.

The dissolved oxygen sensors were calibrated in the laboratory prior to deployments 1 and 2 using gas standards and Winkler titrations of bottle samples taken near the mooring (during deployment and recovery cruises). Sensor output was regressed against the  $pO_2$  of water samples collected at the depth of the sensors. Data from the deployment and recovery cruises were pooled. When a sensor was reused on a subsequent deployment, it was possible (with a single exception) to pool data from two deployments with no significant decrease in the goodness of fit. The average residual error of the regression was  $3 \pm 2 \mu M$  (range of 1.1 - 6.3  $\mu M$ ). Oxygen sensor drift was negligible (i.e., less than 3  $\mu M$  over the course of the 70-106 day deployment period).

The subsurface moored instrument array (Figure 1) included eight MVMS units at nominal depths of 14, 23, 43, 62, 81, 101, 120, and 160 m; BOMS [*Smith et al.*, 1991] at 34, 54, and 72 m; and bioluminescence moored systems, or BLMS [*Swift et al.*, 1988], at 34 and 72 m. The 72-m depth BOMS and BLMS were deployed for the latter two deployments only. There were no MVMS data from 120 m for the first deployment because of a data tape failure. There are some gaps in the time series for various sensors due to either sensor or system malfunctions. These are apparent in the time series presentations of the data set (e.g., Figures 8-12). The BOMS collected downwelling irradiance (wavelengths of 410, 441, 488, 520, and 560 nm), upwelling radiance (wavelengths of 410, 441, 488, 520, and 683 nm), temperature, pressure, and tilt data.

Shipboard bio-optical and conductivity-temperature-depth (CTD) profile data including temperature, conductivity, beam transmission at 660nm, stimulated chlorophyll fluorescence, PAR, and 12 spectral bands of downwelling and upwelling irradiance were collected in the vicinity of the mooring near the times of instrument deployment and recovery [see *Smith et al.*, 1991; *Marra et al.*, 1992]. In addition, chlorophyll *a* and phaeophytin *a*, particulate absorption spectral, and pigment (HPLC analysis [see *Bidigare et al.*, 1989]) and primary production ( $^{14}C$  method) analyses [*Marra et al.*, 1992] were done using discrete water samples.

Meteorological sensors mounted on a surface buoy measured atmospheric pressure, wind speed and direction, air temperature, near surface sea temperature, relative humidity, and shortwave solar radiation [*Dean and Beardsley*, 1988; *Weller et al.*, 1990]. The meteorological data (sampled at 7.5-min intervals) were used to determine the fluxes of momentum, and heat across the air-water interface. Wind stress and heat fluxes were computed using the procedures of *Liu et al.* [1984] and the drag coefficients of *Kondo* [1975] using the algorithms provided by *Liu et al.* [1984].

Time series data presented here have been band-passed (low frequencies passed) using a Gaussian window (either 2 or 24 hours). The autospectra of several physical and bio-optical variables have been determined for each of the deployment periods using standard signal processing techniques. The data records for each variable were divided into overlapping ensembles of 8192 points (corresponding to 22.76 days) which increased the confidence of the spectral estimates while still allowing examination of lower-frequency (i.e., mesoscale) events. Spectra were smoothed at frequencies greater than the semi-diurnal frequency using band averaging. The diurnal (D), semi-diurnal (SD), and local inertial (I; period of 21.5 h) frequencies have been indicated (e.g., Figures 21-25). The two components of the current data represent a vector time series and have been combined and then resolved into clockwise (CW) and counterclockwise (CCW) components [e.g., *Gonella*, 1972]. This procedure is used to evaluate inertial motion energetics as energy levels are characteristically greater for the CW component in the northern hemisphere. Further details may be found in *Dickey et al.* [1990a,b, 1991]. The later use of the terms clockwise and counterclockwise for rotating mesoscale features should not be confused with this rotary spectral nomenclature which applies to local current measurements at the mooring site.

The vertical and horizontal temperature structure in the vicinity of the mooring was sampled during a few time periods with expendable bathythermographs (XBT's) and airborne expendable bathythermographs (AXBT's) [*Chai et al.*, 1991]. The XBT observations were taken prior to mooring deployment and recovery operations along 70°W from ~39°N to ~33°N. Regional AXBT surveys were conducted in the general region as part of the Northwest Atlantic Regional Energetics Experiment (REX) [*Mitchell et al.*, 1985, 1988, 1990; *Dastugue et al.*, 1988].

A data set derived from TIROS-N/NOAA series AVHRR (Advanced Very High Resolution Radiometer) satellite observations of infrared radiation (~1.1 km resolution) was used to attempt to identify mesoscale features using sea surface (brightness) temperature images. Only a few of the AVHRR images were directly useful because of persistently cloudy conditions [*Chai et al.*, 1991]. However, sea surface temperature maps (provided by the NOAA Ocean Services Unit) based on composite (3-day average) data sets derived from ship and AVHRR satellite observations proved useful for identifying the trajectory of the Gulf Stream, major eddies, and warm outbreak features (Figure 2).

Sea surface elevation data were obtained during the Navy's Geosat Exact Repeat Mission (ERM) which spanned the period November 1986 through December 1988 [*Porter et al.*, 1990]. Unlike the AVHRR data, the altimetry data products are virtually unaffected by cloud cover and can be used for coarse time series analysis of mesoscale features in the region of interest. In addition, altimeter data reveal subsurface features which are not always manifest in near surface temperature. The details of the methodology involved with the utilization of Geosat data for sea surface height and residual geostrophic currents are outlined elsewhere [e.g., *Cheney et al.*, 1987; *Zlotnicki et al.*, 1989; *Vazquez et al.*, 1990; *Vazquez*, 1991] and information concerning the present utilization of Geosat data are given in *Chai et al.* [1991]. Because of a lack of a geoid model, the mean sea level, computed as the 2-year average SSH (and thus the signature of the Gulf Stream), is removed [*Vazquez et al.*, 1990]. For our work, a smoothing window of 46-km latitude and 27-km longitude was used. The scene was used to create 10-day maps of the residual sea level with 0.25° latitudinal and longitudinal resolution. It should be noted that there is some as yet undetermined amount of error in the SSH data, apparently related to orbit error (V. Zlotnicki, personal communication, 1991). A chronology of mesoscale features reflected in the residual SSH and geostrophic current data and the composite sea surface

temperature (SST) data is given in *Chai et al.* [1991]. The mesoscale features are best demonstrated in the color SSH maps of *Chai et al.* [1991], which are not shown here because of publication expense.

Generally, we note good correspondence between features in sea surface elevation and sea surface temperature. The dates shown in the panels of Figure 3 are at the midpoints of the 10-day sampling intervals.

Our original motivation for using Geosat data was to aid in the interpretation of the mooring data set, particularly to qualitatively assess the role of advection. For clarity, it should be noted that the mooring measurements are Eulerian and that the temporal variations measured at the mooring site result from both temporal changes in a property (say, temperature  $T$ ) within an observed water parcel at the site ( $dT/dt$ ) and the flow of water masses within a spatial gradient (e.g.,  $u\partial T/\partial x$ ) or for one-dimensional flow (e.g., eastward), the mooring measures local changes according to

$$\partial T/\partial t = dT/dt - (u\partial T/\partial x)$$

The last term on the right-hand side, the advection term, can be very important yet it cannot be easily estimated (this is a classical physical oceanographic problem). For this reason, we have utilized available satellite data sets to assist in our interpretation of the mooring data and more particularly to make rough inferences concerning the possible contributions by the advection terms to the mooring signals.

As indicated earlier, sea surface temperature maps were of limited value. Nonetheless, many of the features noted in these maps were corroborated by the Geosat SSH and residual geostrophic (RG) current maps. However, some features were discernable only with the Geosat data, because of sampling, weakness in temperature gradients, or the lack of surface temperature expressions. A comparison of RG currents derived from Geosat data with direct current measurements at a given location has several inherent problems. Specifically, the RG currents do not include the long-term (2-year) mean. In addition, the spatial and temporal scales of the determinations are by necessity quite coarse. And as mentioned earlier, there is some as yet undetermined correlated along-track error which is probably most detrimental to current direction determinations. The direct mooring current measurements are representative of a single point and mooring motion causes some error; however, these measurements are relatively accurate and subject to little bias.

Despite the difficulties with comparing currents derived from the two very different methodologies, there have been a few encouraging intercomparisons [e.g., *Picaut et al.*, 1990; *Willebrand et al.*, 1990]. The directly measured local currents include contributions from both local wind-driven and geostrophic components. The wind-driven currents were modeled with a mixed layer model (level 2 1/2 of *Mellor and Yamada* [1982]). Measured atmospheric parameters were used as input. The horizontal kinetic energy, determined by subtracting the wind driven component from the directly determined (current meter) component for a depth of 14 m is shown on the same time series plot as the Geosat derived RG current (Figure 4). We obtain a coefficient of determination value of  $r^2=0.74$  between the two determinations of geostrophic kinetic energy. A time series of current vectors based on this analysis (not shown) indicates a bias in direction (roughly 45°) to the right of the Geosat current vectors. The explanation for this is not obvious; however, it is not surprising considering the many differences (especially sampling scale disparities) and uncertainties in both of the methods. Nonetheless, we found that Geosat data were very useful for identifying mesoscale features in the vicinity of the mooring and that Geosat derived current speeds (accounting for wind-driven component) were in reasonable agreement with direct current measurements. Details

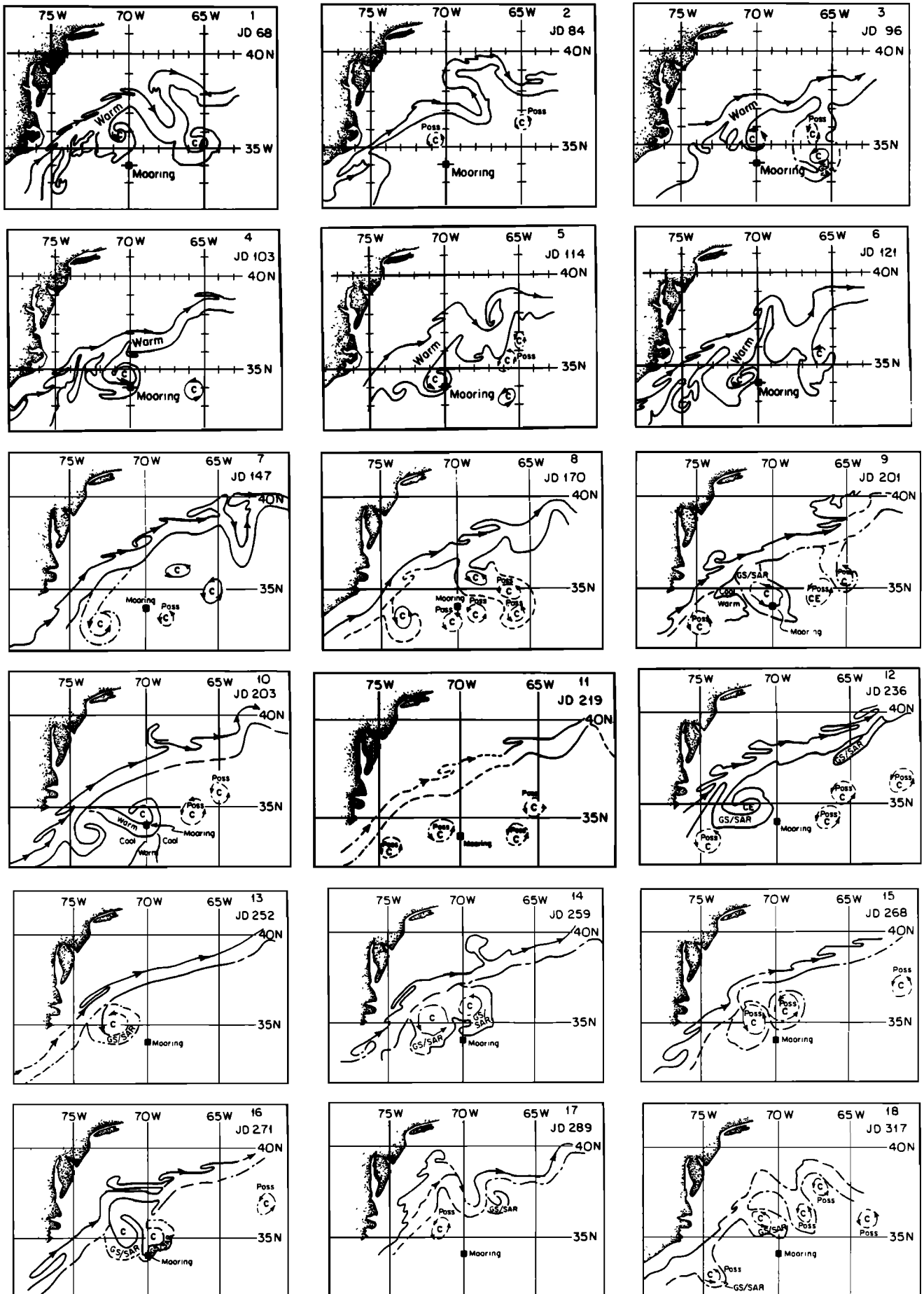
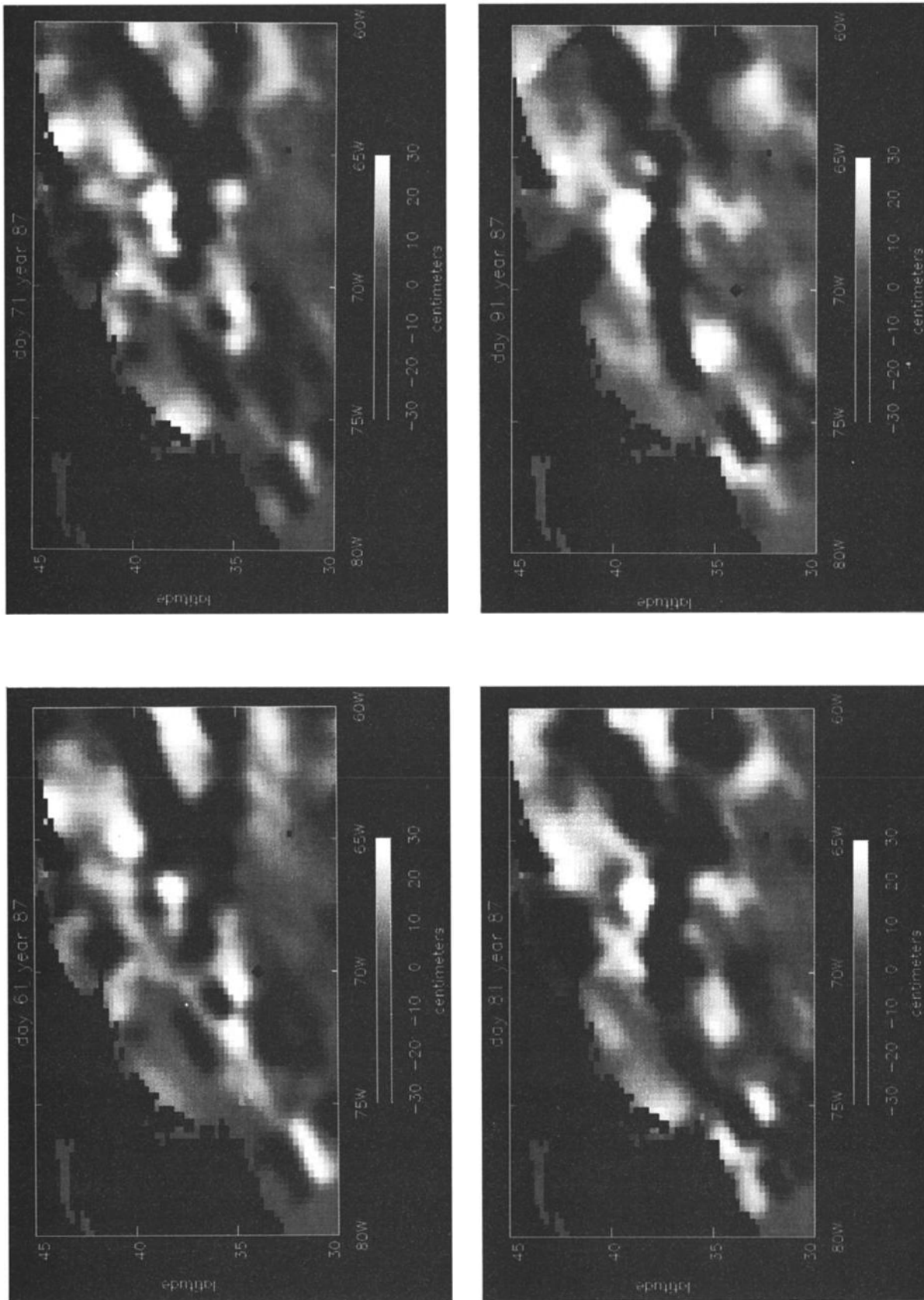


Fig. 2. The region of the Biowatt study and the location of the Biowatt II mooring. The path of the Gulf Stream, its associated warm outbreaks, and cold core rings as determined from sea surface temperature data are shown. Individual panels are shown to indicate the primary advective features representative of 18 individual time periods (as indicated in Table 1).



**Fig. 3.** Sea surface height maps for the region of  $30^{\circ}\text{N}$ - $45^{\circ}\text{N}$  and  $60^{\circ}\text{W}$ - $80^{\circ}\text{W}$  computed using Geosat altimetry data. The 2-year mean sea level (and thus the primary signature of the Gulf Stream) is removed prior to the calculations, which utilize 10 days of data for each map. The purpose of these scenes is primarily to identify mesoscale features. The dates shown in the panels are at the midpoints of the 10-day sampling intervals. The diamond symbol indicates the mooring site, and the square symbol indicates the island of Bermuda.

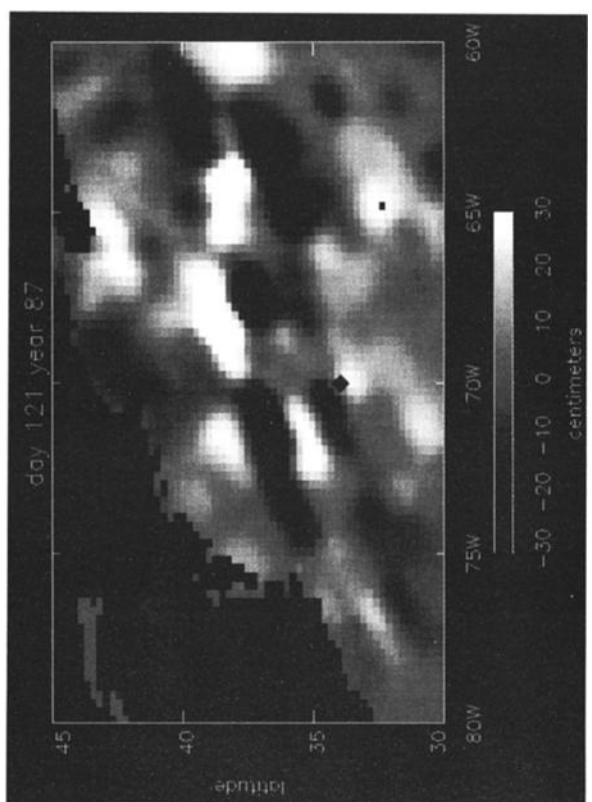
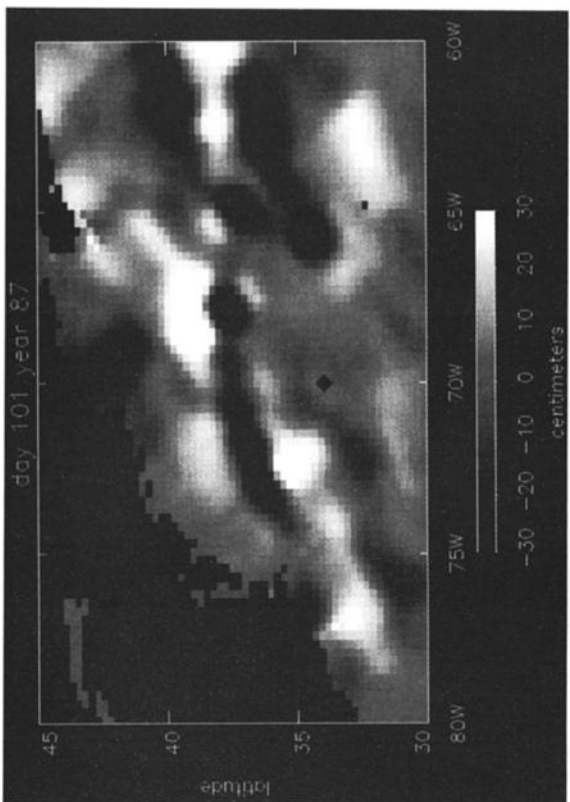
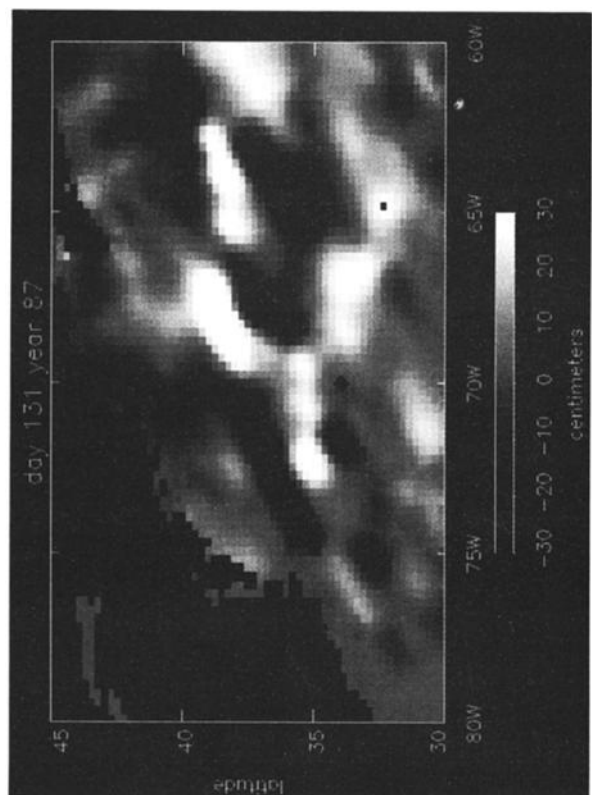
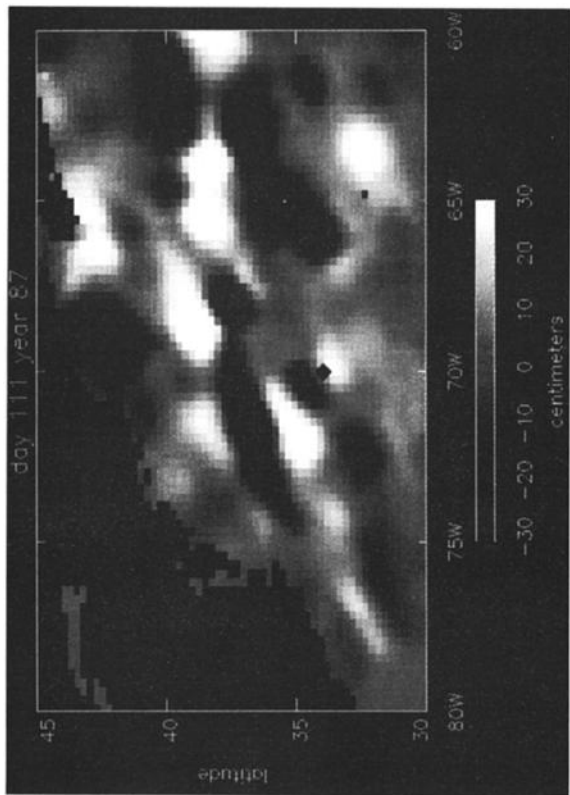


Fig.3 (continued)

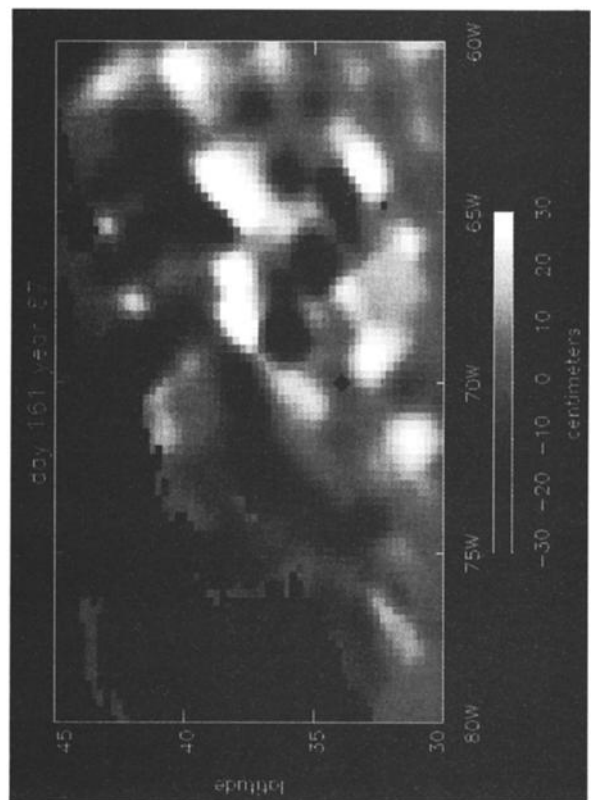
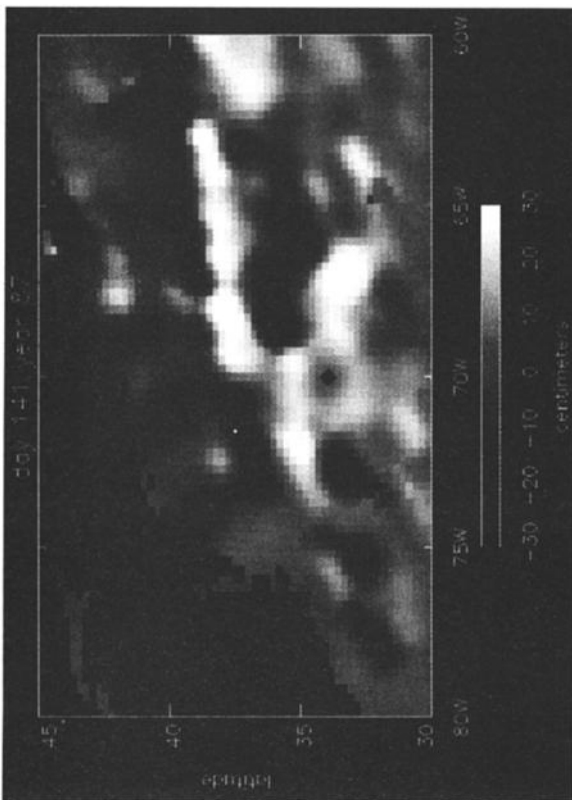
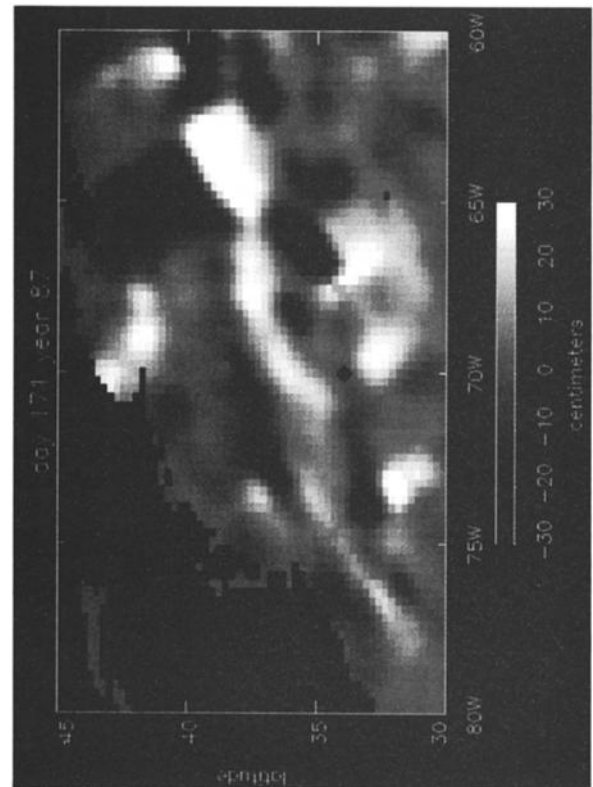
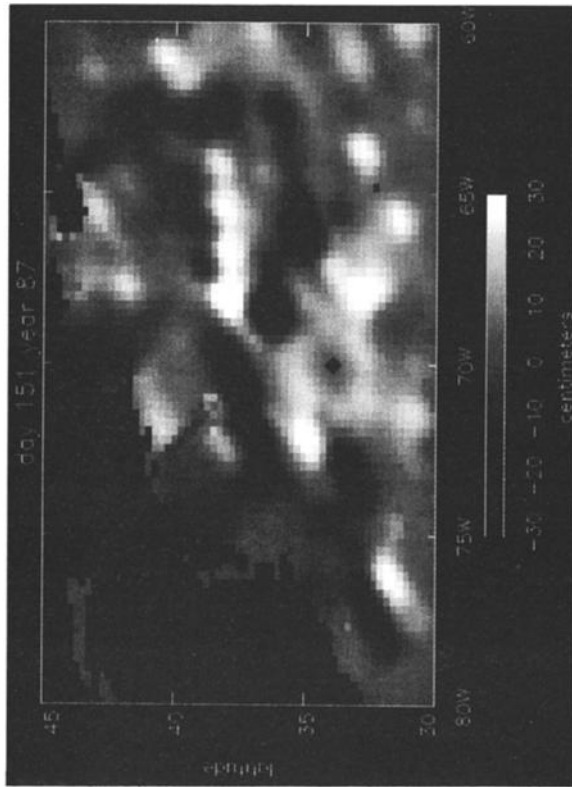


Fig.3 (continued)

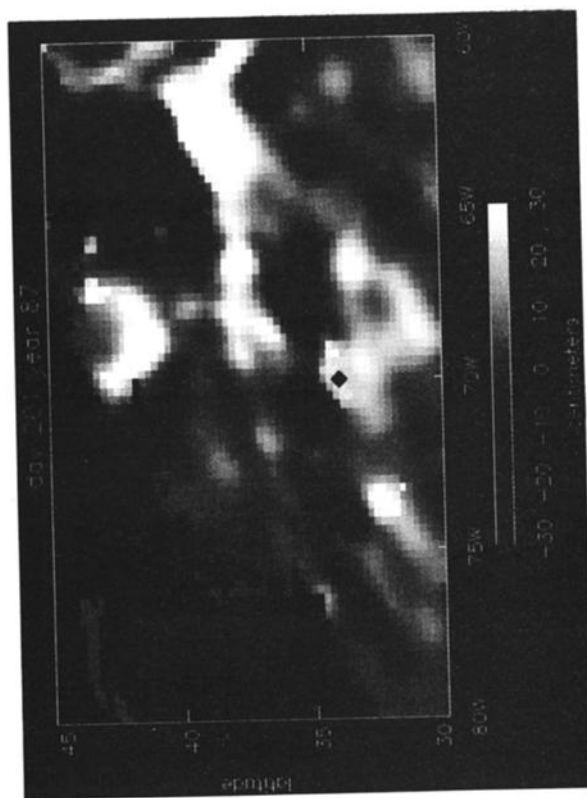
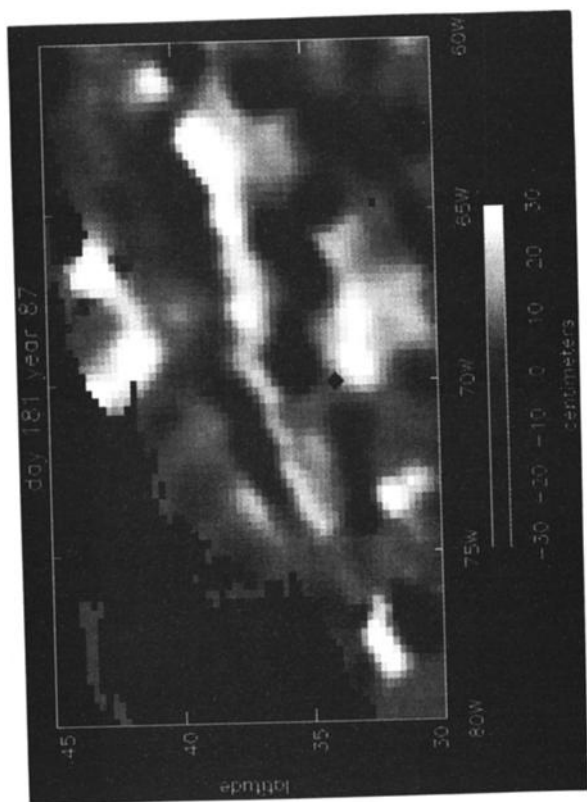
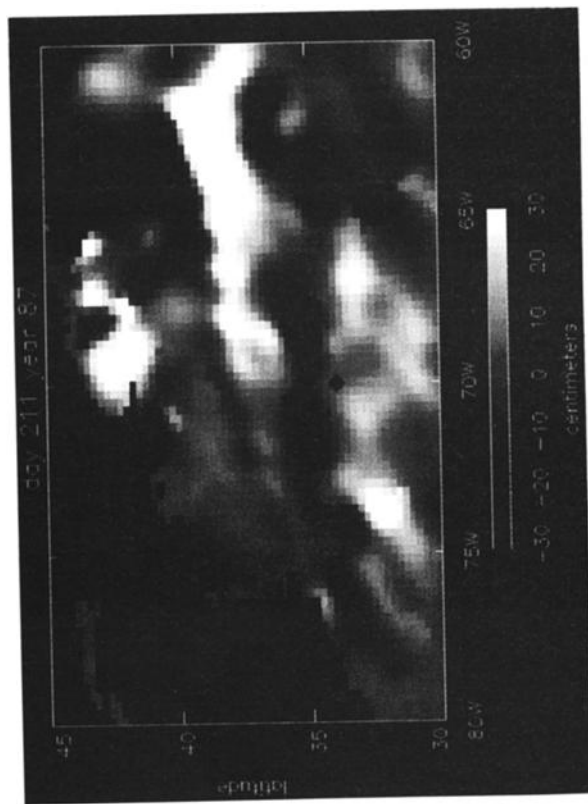
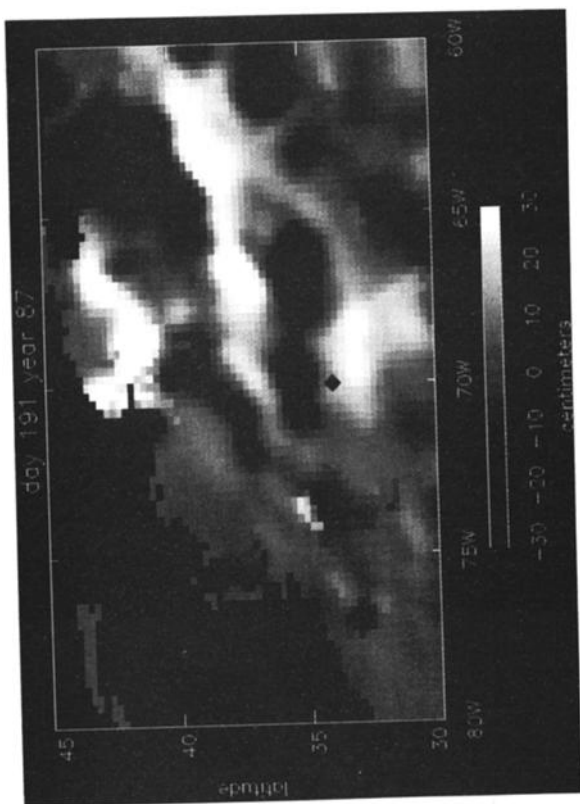


Fig.3 (continued)

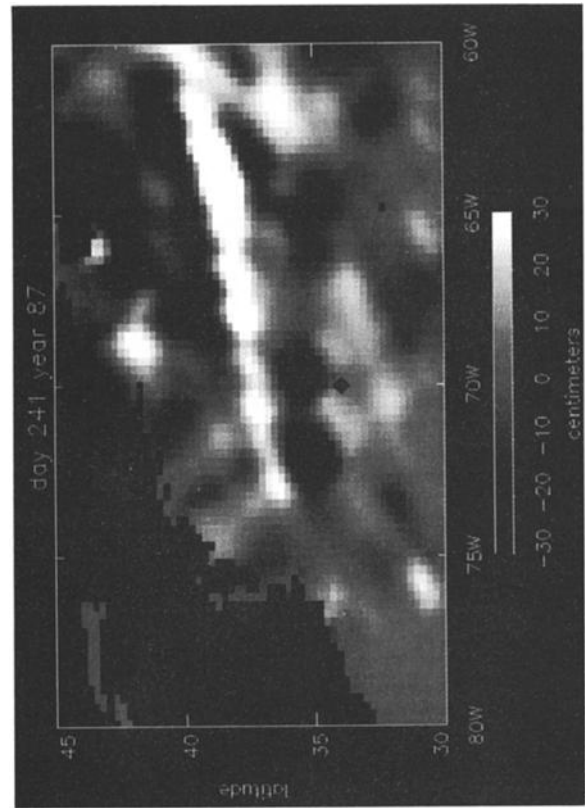
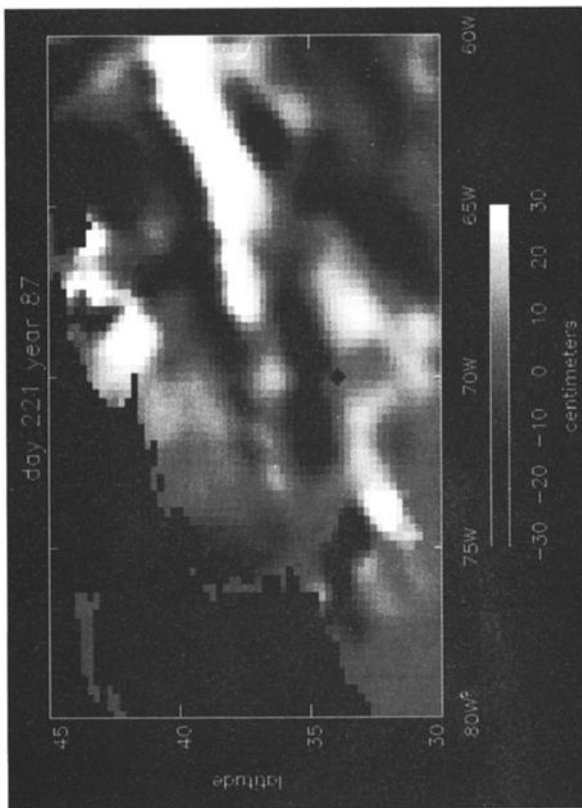
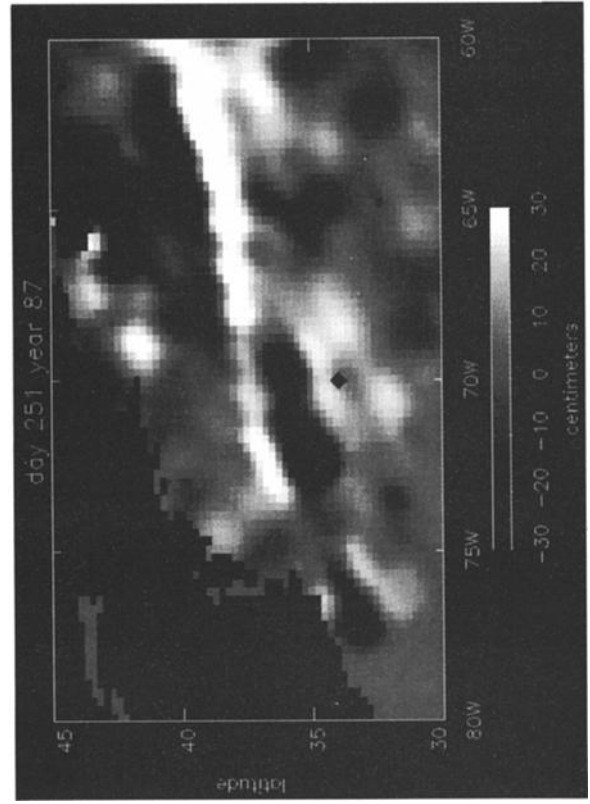
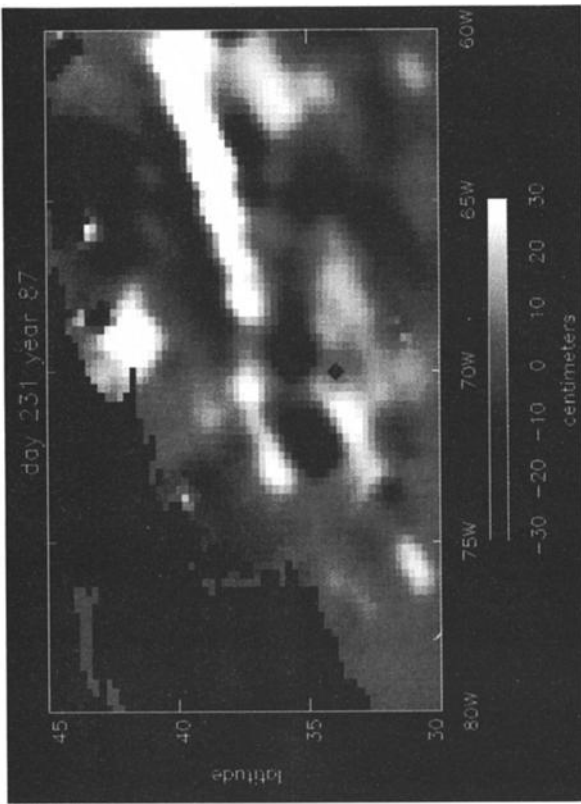


Fig.3 (continued)

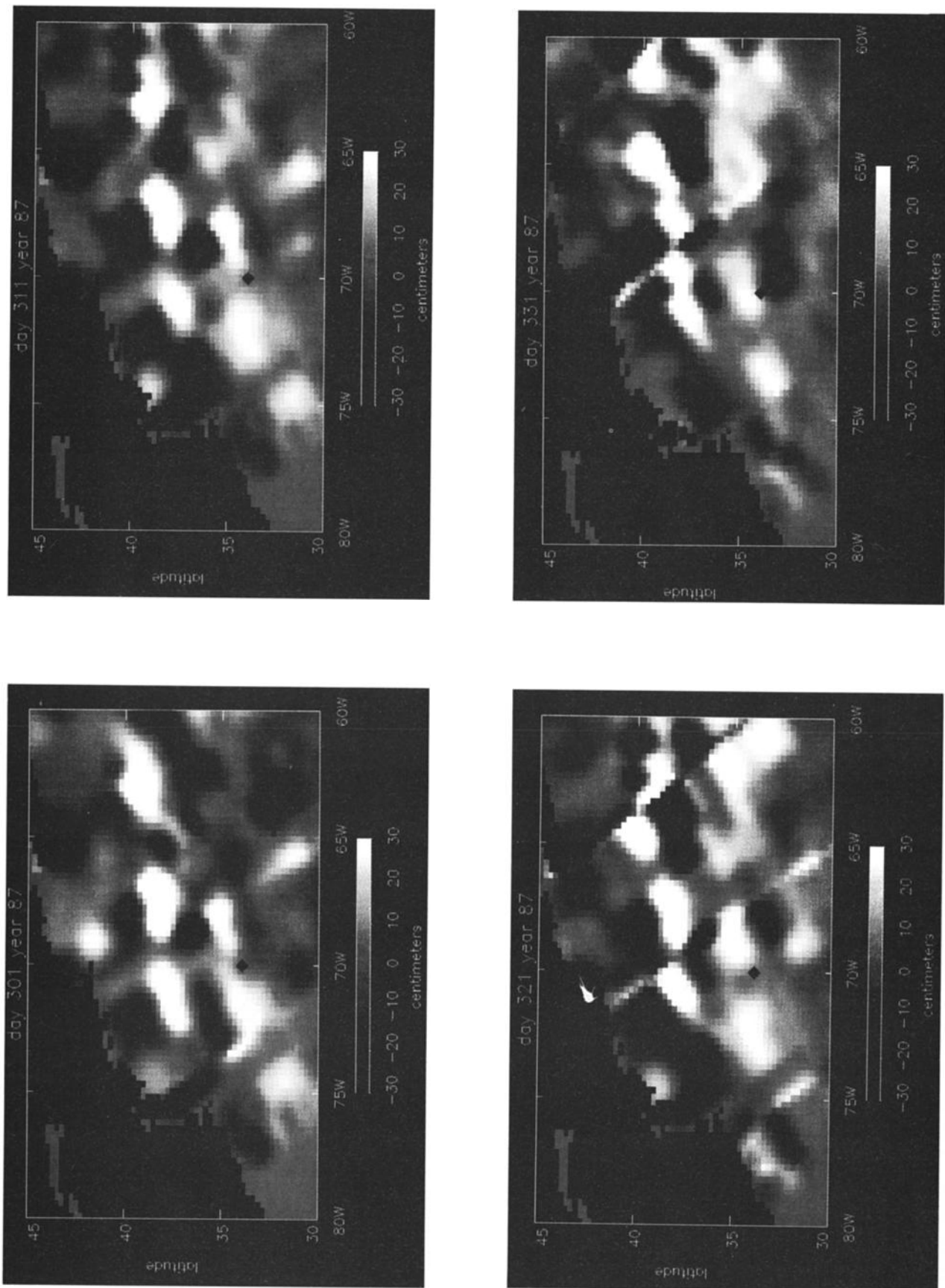


Fig.3 (continued)

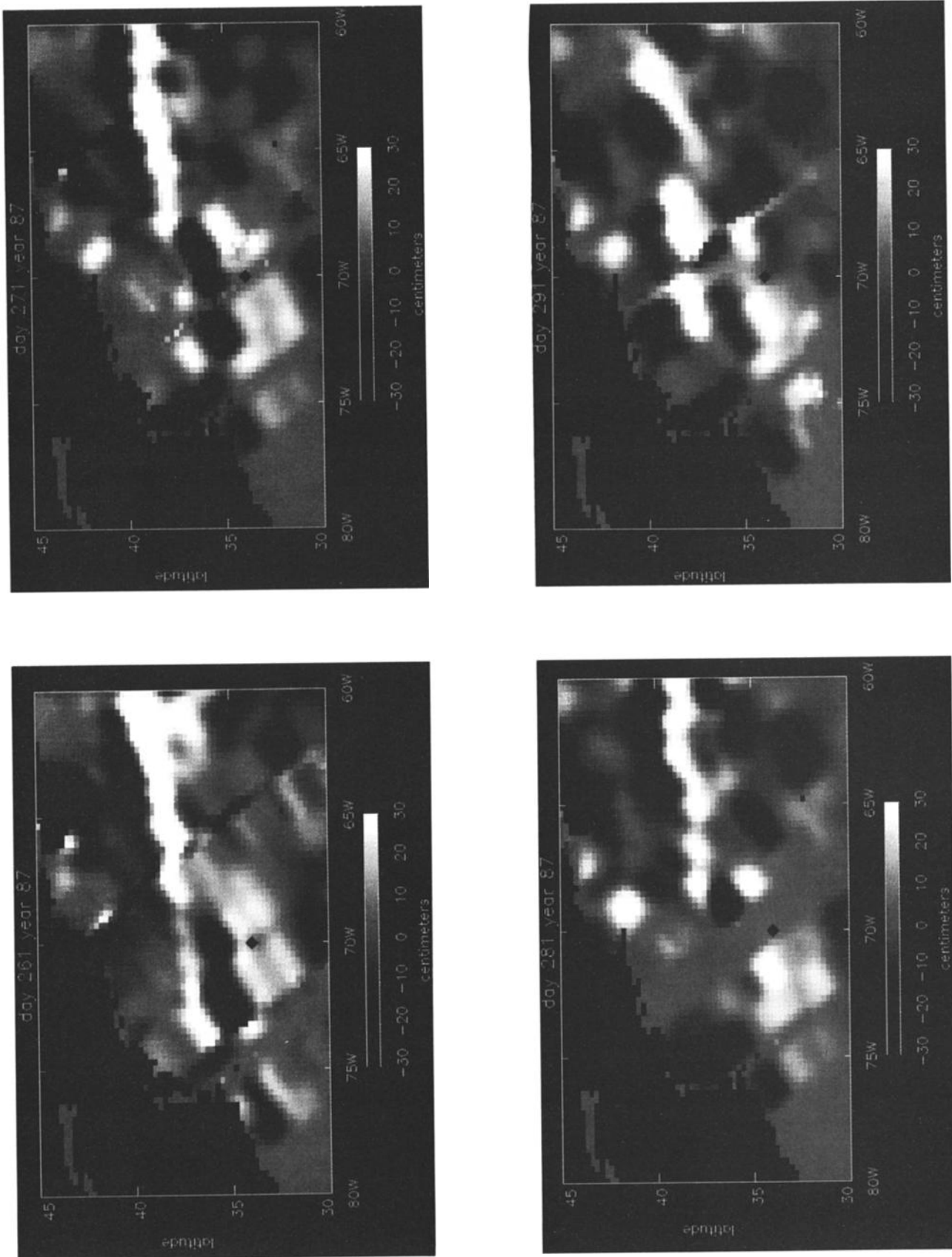


Fig.3 (continued)

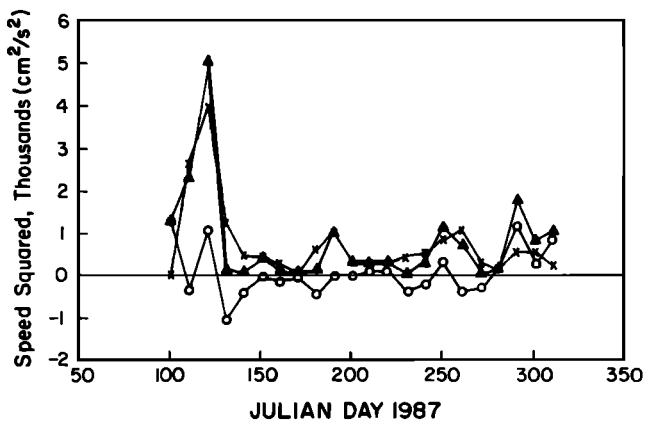


Fig. 4. Time series of horizontal kinetic energy of geostrophic current derived from Geosat elevation data (crosses) and the kinetic energy computed by subtracting model wind driven current (interpolated to 14 m) from the directly measured current at 14 m (triangles). The difference between these time series is also shown (circles).

concerning this aspect of the present work are presented in *Chai et al.* [1991].

### 3. OBSERVATIONS

The region and specific mooring site in the Sargasso Sea (34°N, 70°W; see Figure 1) of the present observations has been the subject of several studies [see *Dickey et al.*, 1991]. The region is characterized by oceanic and atmospheric conditions including (1) daily and seasonal heating cycles, (2) episodic strong wind forcing and cloudy conditions associated with atmospheric frontal passages and on occasion hurricanes, (3) internal gravity waves and tides, (4) small-scale mixing events associated with atmospheric forcing and current shears, and (5) advectively forced variability such as cold core rings and warm water outbreaks associated with the Gulf Stream [e.g., *Cornillon et al.*, 1986]. The mesoscale features are of particular interest in the context of time series observations from a fixed mooring, since they are known sources of ecological variability. In addition, these features necessitate the use of complementary data sets which can provide contextual information concerning horizontal variability. An analysis of Geosat data for the period November 1986 to June 1989 by *Le Traon* [1991] indicates that the characteristic time scale of mesoscale variability at our site was about 45 days.

In order to facilitate interpretation, the time series data have been subdivided into 18 observational periods (Table 1), which were selected on the basis of temperature structure, current regime, and bio-optical properties. The lengths of these periods are unequal. In addition, maps of the SSH field (28 maps at 10-day intervals), based on altimetry data collected from Geosat [*Chai et al.*, 1991], are used to aid in the analysis (Figure 3).

The seasonal physical forcing and response for the present study are summarized in Figures 5, 6, and 7. The three deployment periods coincided with roughly distinct oceanic regimes. The first deployment (JD 60-130) presents a late wintertime to late springtime situation, the second deployment (JD 136-242) presents a late springtime to late summertime situation, and the third deployment (JD 243-327) presents a late summertime to late fall situation. The first and third deployments are marked by considerably greater variability in the atmospheric forcing associated with synoptic-scale weather systems than the second deployment as evident in time series of atmospheric pressure, wind stress, incident radiation, and net heat flux. The second deployment period is relatively quiescent compared with the others in terms of the upper ocean response

as reflected in mixed layer depth, current speed, and mixing time scale. The mixing time scale is computed using the relation  $T_M = 2 \times \text{mixed layer depth} / (2 \times \text{water friction velocity})$ , where the water friction velocity is the square root of the quotient of wind stress and water density [e.g., *Denman and Gargett*, 1983]. The criterion for the mixed layer depth is somewhat arbitrarily chosen to be the depth at which temperature has decreased by 0.5°C with respect to surface temperature. Criteria of 0.1°C through 0.5°C have also been applied to the data set, and the resulting mixing time scales are about the same except during deployment 3, when the mixed layer based on the 0.1-0.2°C criterion remains near 20 m, while the 0.4-0.5°C criterion indicates a major deepening event. This analysis suggests that multiple vertical temperature steps are present in the fall period. It is likely that even weak vertical step structures in density may influence the actual time scales relevant to the phytoplankton [e.g., *Denman and Gargett*, 1988]. The purpose of this analysis is primarily to enable a comparison of relative time spent by a particle in the mixed layer. Others have examined the use of biomarkers and photoadaptation characteristics of phytoplankton for estimating the rate of vertical mixing and for examining how phytoplankton integrate environmental fluctuations. The fundamental concept, as forwarded by *Cullen and Lewis* [1988], is that phytoplankton in a mixed layer will exhibit a vertical gradient with adaptation to ambient light intensities if the mixing time scale is longer than the photoadaptive time scale. On the other hand, the phytoplankton properties will be uniform with depth if the mixing occurs within a time scale shorter than that of photoadaptation. *Cullen and Lewis* [1988] report that in response to bright light, fluorescence is depressed on a time scale of less than an hour and that photosynthetic capacity can recover over many hours to a high level characteristic of an adapted state. The present data set may be used for similar detailed analyses in the future. The mixing time scales observed during the present experiment are greatest during the first period ( $>10^4$  s or  $\sim 3$  h) through  $\sim$ JD 90, then they remain about an order of magnitude smaller ( $\sim 15$  min) until the final deployment when they again approach values near  $10^4$  s. Thus, both photoadaptive and mixing processes may be relevant at times.

Incident solar radiation and net heat flux are greatest during the second deployment. The major seasonal effects are the rapid shoaling of the mixed layer during the first deployment and the late fall deepening of the mixed layer during the third deployment. Mesoscale advective features including warm outbreaks and cold core rings influence the time series, causing varying degrees of perturbations to the seasonal cycle on time scales of days to a couple of weeks. These events are most apparent in the temperature time series (Figure 6), but also at times in increased currents (Figure 8). The sea surface temperature and height maps provide further evidence of mesoscale activity (Figures 2 and 3).

The incoming shortwave radiation is modulated by clouds and increases as expected from the late winter to early springtime period and declines in the fall. The latent heat flux dominates the heat loss terms, with the next most important term being the net longwave radiation. The latent heat flux term can be 2 to 3 times as great as the longwave term. The mooring site is near the geographic location marked by the greatest annual heat loss to the atmosphere in the North Atlantic [*Bunker*, 1976]. The net heat flux exhibits a diurnal modulation and has a peak value of  $\sim 800 \text{ W m}^{-2}$  and a maximum heat loss (occurring during the late winter to early spring) of nearly  $600 \text{ W m}^{-2}$ . The daily mean net heat flux increases through the first deployment and decreases during the fall due to the seasonal cycle. The present meteorological data are consistent with the climatological data reported by *Bunker* [1976] and other data taken with sensors comparable to those used for the present experiment at the

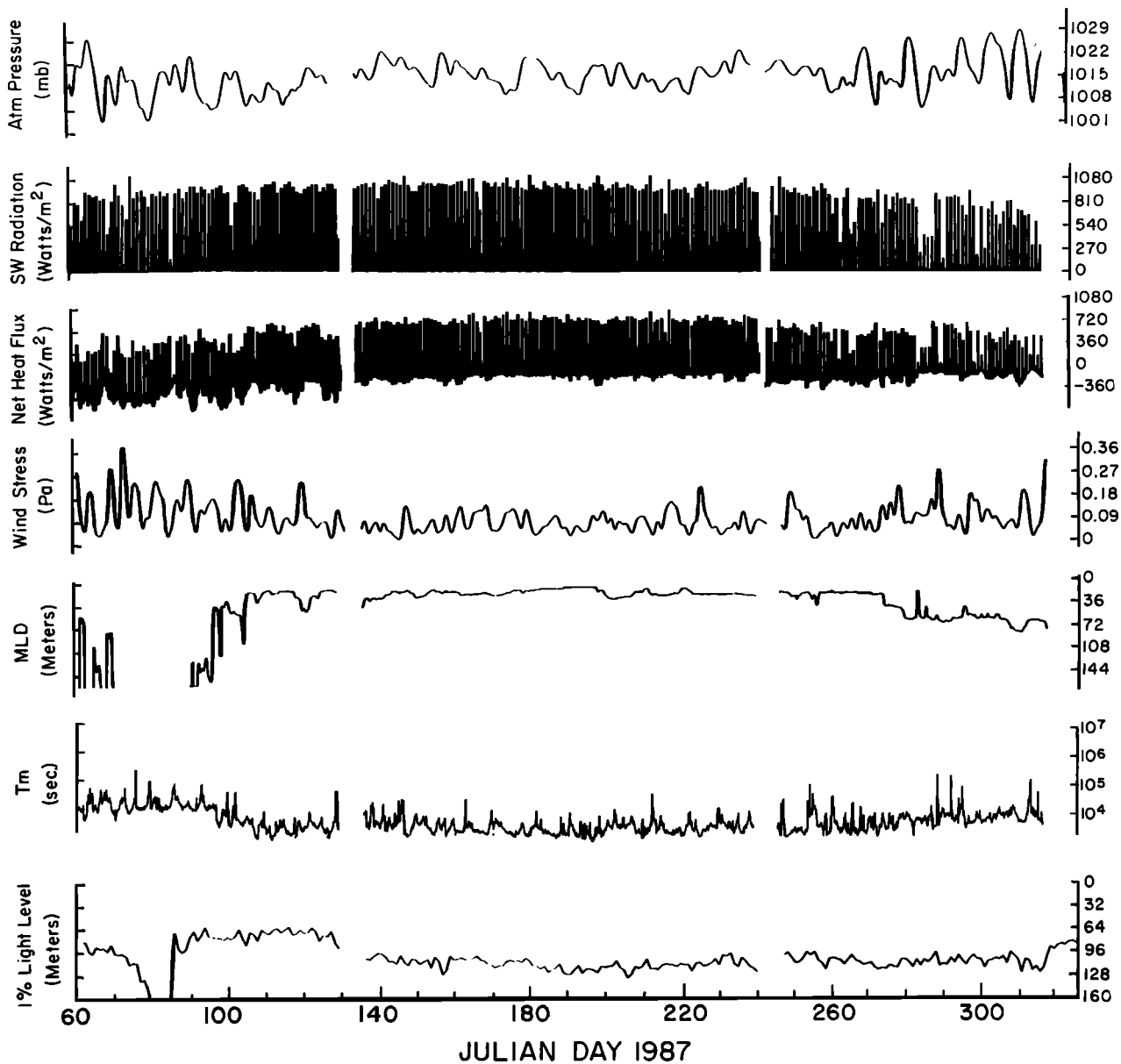


Fig. 5. Time series (2-h filter) of atmospheric pressure in mbar, shortwave solar radiation in  $W m^{-2}$ , net heat flux in  $W m^{-2}$ , wind stress in Pa, mixed layer depth in meters, mixing time scale in seconds, and depth of 1% light level in meters.

mooring site [Deser *et al.*, 1983]. Further details concerning the meteorological data set may be found in Dickey *et al.* [1990a,b, 1991].

General descriptions of the results of each of the three deployments are given below. The events of the first six periods (deployment 1) have been described by Dickey *et al.* [1991]. The detailed sequence of events for the latter 12 periods follows the general summaries and readers less interested in the specifics may wish to proceed to the discussion section after reading the summaries.

*Summary of Deployment 1: Julian Days 60-130, March 1 to May 10, 1987*

The seasonal mixed layer is generally quite deep (at times >160 m) during the first part of the deployment, but warm outbreak waters derived from the Gulf Stream appear to advect through the mooring site as indicated by the variation of the mixed layer depth and the isotherms within the upper 160 m

(Figures 6 and 7). Cornillon *et al.* [1986] describe warm outbreaks as large bodies of Gulf Stream water, which detach from the Gulf Stream and then exist as well-defined entities. They describe outbreak features which form within a few days, persist for ~10 to 20 days, and have dimensions of the order of 100 to 200 km. The sea surface temperature map for JD 68 shows such outbreaks to the northwest and northeast of the mooring site (Figure 2). The SSH (Figure 3) derived from the Geosat data for this period (JD 61 and 71) also indicates the outbreaks and cold core rings (near 35.5°N, 71°W and 35.0°N, 65°W) to the northwest and northeast of the site. It is likely that the mooring, located at a position near a boundary between warm outbreak waters and Sargasso Sea waters, sensed the differing waters (cooler Sargasso Sea water and warmer Gulf Stream outbreak water) as they meandered about the mooring site. An XBT section (not shown) also confirms this interpretation [Chai *et al.*, 1991].

The first deployment is characterized by strong and variable wind forcing associated with the passage of atmospheric low

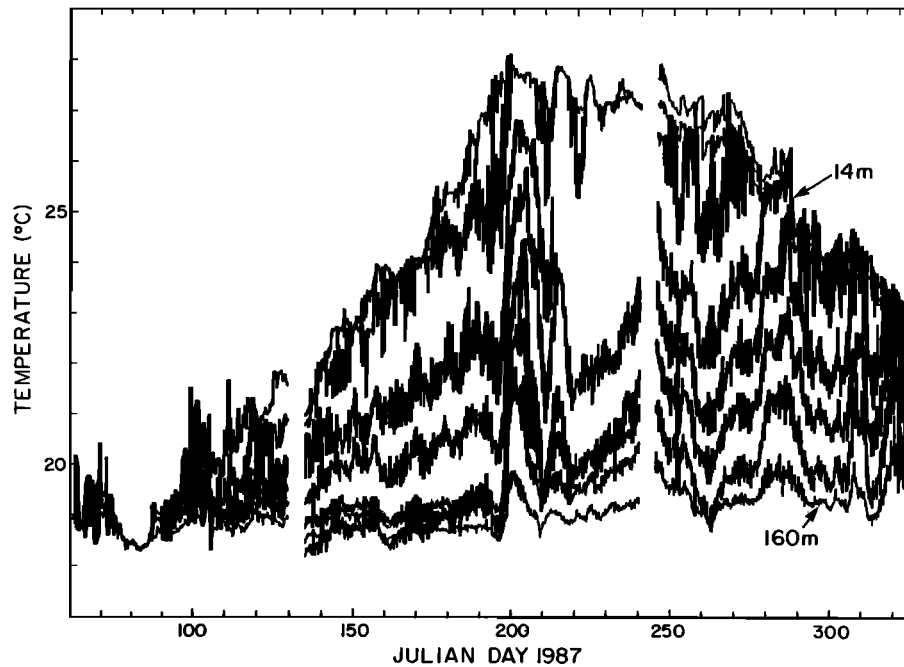


Fig. 6. Time series (2 h filter) of temperature for eight depths in the upper 160 m (top curve is from 14-m record, and bottom curve is from the 160-m record). Note that no data were collected for the 43-m depth during the period JD 213-241 of deployment 2.

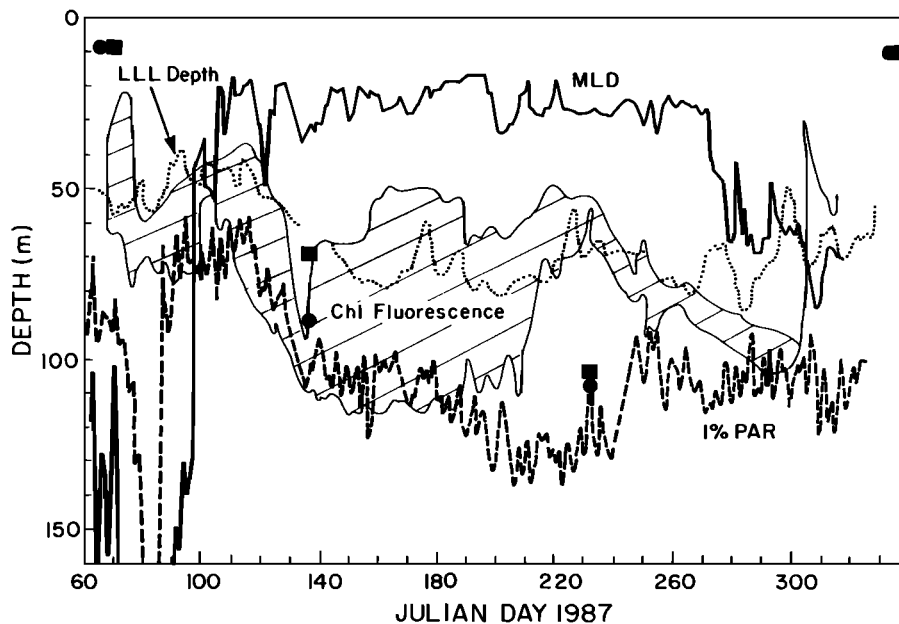


Fig. 7. Time series (based on daily averages) of the depth of the 1% light level (1% value of surface PAR), the depth of the contour of the low light level (LLL) for a PAR value of  $2.1 \times 10^{19}$  quanta  $m^{-2} s^{-1}$  ( $\sim 35 \mu E m^{-2} s^{-1}$ ), and the mixed layer depth. The mixed layer depth is defined here as the depth at which the temperature is  $0.5^\circ C$  cooler than the surface temperature. The region of the chlorophyll maximum is indicated. The envelope, by definition, encompasses values of chlorophyll in excess of  $0.40 \mu g$  Chl  $a L^{-1}$ . Depths of the chlorophyll maxima and  $0.25 \mu M$  (or greater if at surface) nitrate levels as determined from discrete water samples obtained from inter-deployment CTD/rosette casts are indicated as circles and squares, respectively. At times, the mixed layer depth and the 1% light level exceeded 160 m, the greatest depth of our observations.

pressure systems (Figure 5). The solar insolation generally increases because of the seasonal progression from winter to spring (Figure 5). The currents are generally more intense and variable during this deployment than the other two deployments, in part because of mesoscale advective features reflected in subsurface temperature and currents (Figures 6, 8,

13, and 14) and in part because of the more intense local wind stresses (Figure 5). There are also considerable variations in bio-optical properties (PAR, beam attenuation coefficient, chlorophyll fluorescence, and dissolved oxygen; Figures 9, 10, 11, and 12), possibly because of the advection of water masses with differing biomasses and histories. Large excursions in the

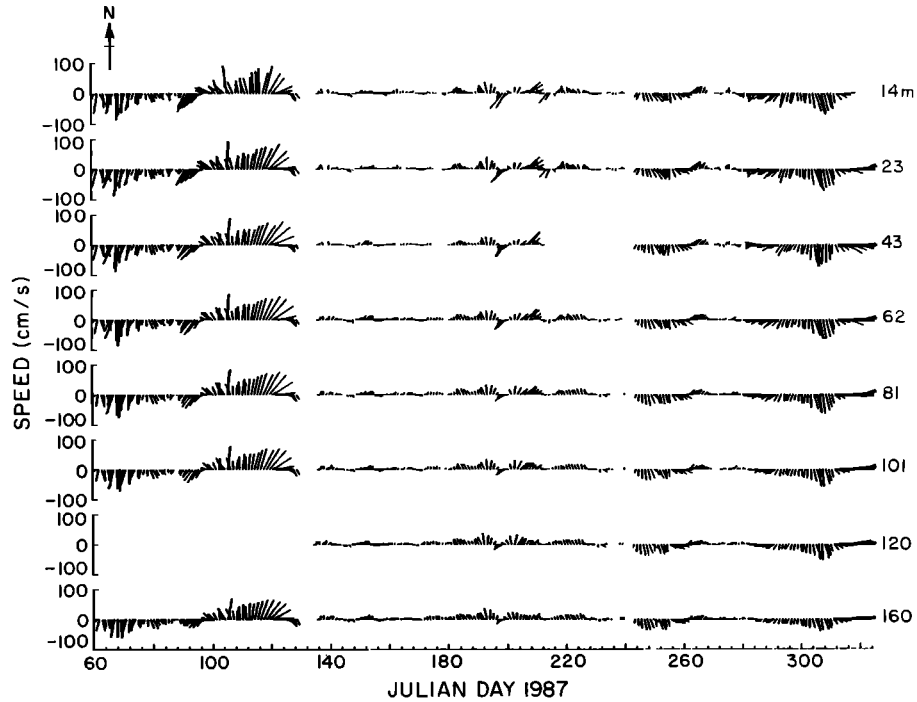


Fig. 8. Time series of daily averaged vector currents ( $\text{cm s}^{-1}$ ).

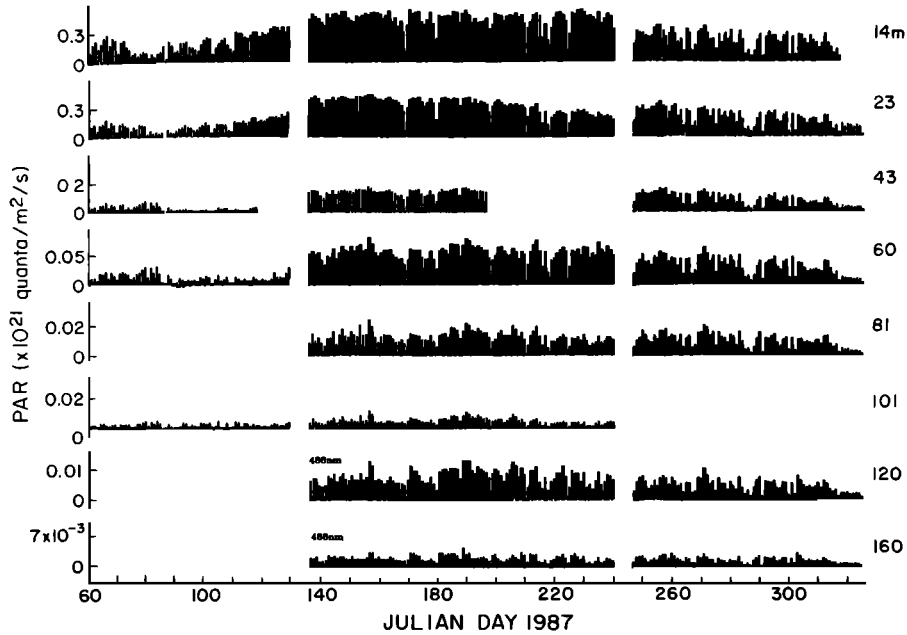


Fig. 9. Time series (2 h filter) of PAR (in units of  $10^{21}$  quanta  $\text{m}^{-2} \text{s}^{-1}$ ) and downward irradiance at 488 nm (in units of  $\text{W m}^{-2} \text{nm}^{-1}$ ) in the upper 100 m and at 120- and 160-m depths, respectively.

mixed layer depth and the 1% light level are apparent. The depth of the LLL is  $\sim 50$  m until  $\sim$ JD 110, when it begins to descend to  $\sim 80$  m by  $\sim$ JD 140. The LLL depth tends to track the chlorophyll maximum envelope (Figure 7). This deployment is also particularly biologically dynamic because of the onset of seasonal stratification and the increasing phytoplankton abundance [Dickey *et al.*, 1991; Smith *et al.*, 1991; Marra *et al.*, 1992]. The mixing time scale decreases by about an order of magnitude as the mixed layer shoals. A relatively intense

subsurface chlorophyll maximum is apparent, especially during the latter portion of this deployment (Figures 7 and 18). The depth integrated chlorophyll is relatively great, especially after JD 86, and remains so until  $\sim$ JD 160, when it decreases (see Figure 7b in Marra *et al.* [1992]).

During the earlier portion of the deployment, winter conditions prevail with characteristic elevated nutrient concentrations (see profiles in Marra *et al.* [1992]), as indicated by surface values of nitrate greater than  $0.6 \mu\text{M}$ . Vertical

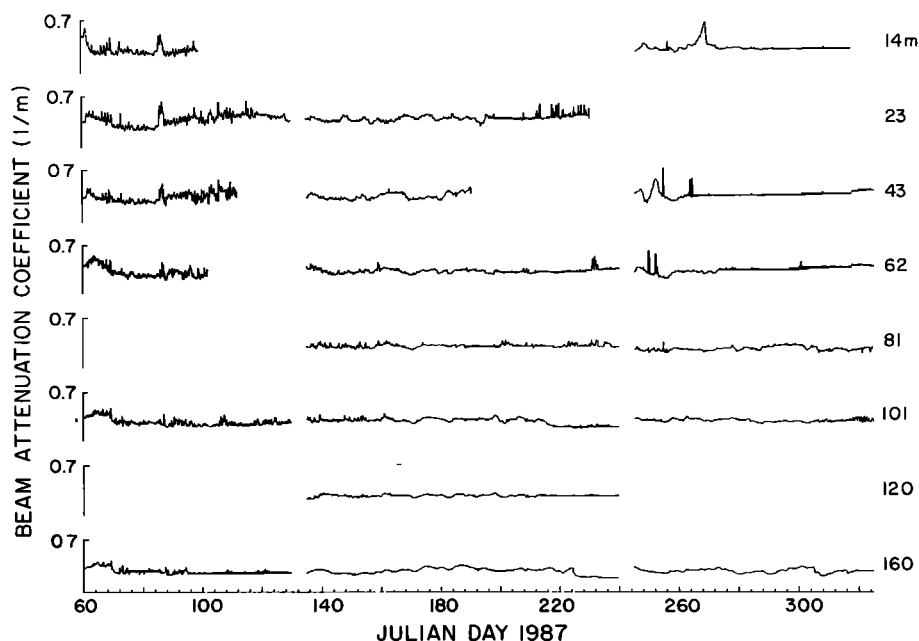


Fig. 10. Time series (2-h filter) of beam attenuation coefficient ( $m^{-1}$ ). Clear water value is  $0.364 m^{-1}$ .

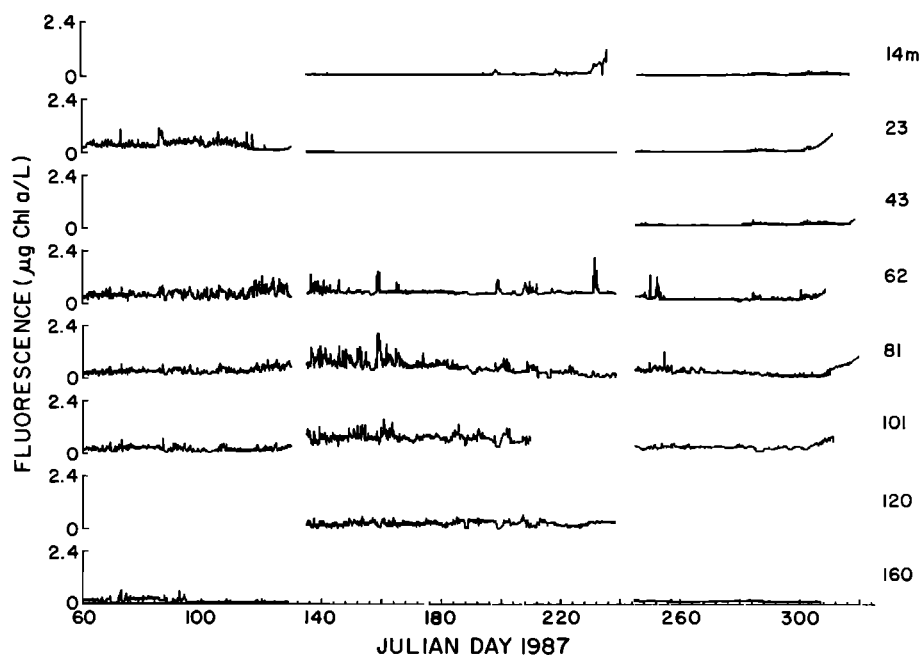


Fig. 11. Time series (2-h filter) of chlorophyll fluorescence ( $\mu g Chl L^{-1}$ ).

profiles of selected accessory pigments are shown in Figure 20 for the wintertime condition (e.g., JD 63-67 from Oceanus cruise OC 1). The principal phytoplankton groups of associated diagnostic marker pigments are indicated in Table 2, along with depth integrated (surface to 200 m) pigment concentrations and accessory pigment-to-chlorophyll ratios (based on data of Bidigare and Ondrusek [1988]). At this time the phytoplankton community (represented primarily by prymnesiophytes, chrysophytes, cryptophytes, prasinophytes, and cyanobacteria) displayed a (pigment) biomass maximum at circa 30 m, with only minor compositional variations in the upper 200 m. In early spring with the onset of stratification, conditions are favorable (sufficient nutrients and light, and

reduced mixing time scales) for a phytoplankton bloom (most likely diatoms [cf. Bidigare et al., 1990]). The bloom probably is responsible for the effect of nearly depleting the surface nitrate and silicate by JD 138-140 (Oceanus cruise OC2). The bloom appears to be advected past the site as warm outbreak waters associated with a ring to the west meanders past the mooring.

With increased stratification and phytoplankton uptake of nitrate, a steep gradient in nitrate is produced along with a strong chlorophyll maximum layer. We define a chlorophyll maximum region or envelope, to encompass values of chlorophyll in excess of  $0.40 \mu g Chl a L^{-1}$ . At this time, the chlorophyll envelope appears to be bound in a rough sense by

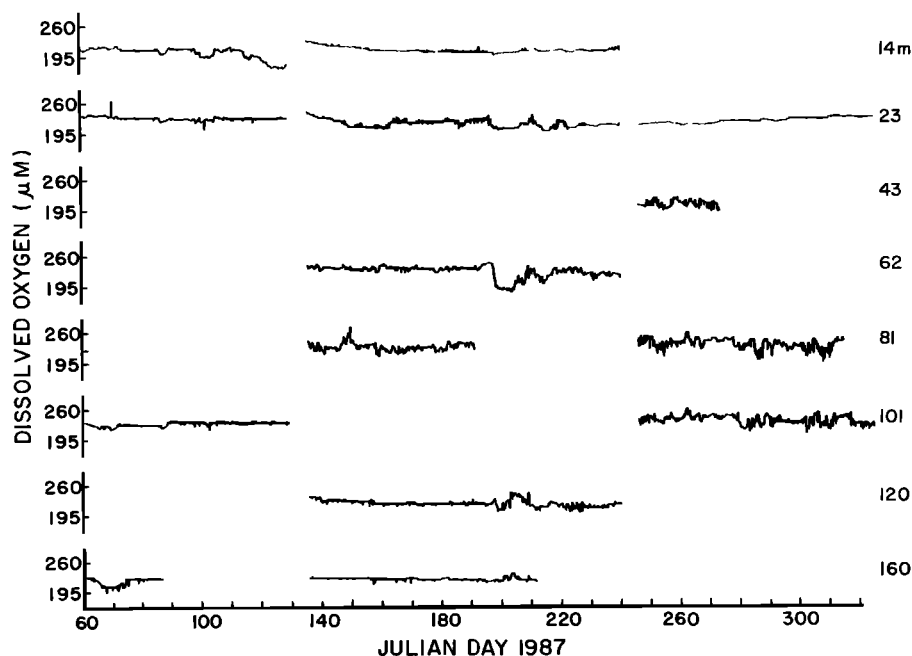


Fig. 12. Time series (2-h filter) of dissolved oxygen concentration ( $\mu\text{M}$ ).

TABLE 2. Seasonal Distribution of Pigment Biomarker Concentrations ( $\text{mg m}^{-2}$ )

Pigment Marker	JD 64 Winter/Spring	JD 138 Late Spring	JD 235 Summer	JD 335 Fall/Winter
"Chlorophyll <i>a</i> " (algal biomass)	53.6	23.2	22.8	43.0
Peridinin (dinoflagellates)	0.0 (0.00)	0.0 (0.00)	0.5 (0.02)	0.0 (0.00)
19'-but-fucoanthin (chrysophytes)	7.8 (0.15)	2.0 (0.09)	2.6 (0.11)	4.6 (0.11)
Fucoanthin (diatoms)	6.3 (0.12)	1.0 (0.04)	0.4 (0.02)	4.0 (0.09)
19'-hex-fucoanthin (prymnesiophytes)	12.0 (0.22)	6.0 (0.26)	4.9 (0.22)	10.2 (0.24)
Prasinanthin (prasinophytes)	3.2 (0.06)	0.0 (0.0)	0.0 (0.0)	1.7 (0.04)
Alloxanthin (cryptophytes)	1.5 (0.03)	0.0 (0.0)	0.0 (0.0)	1.6 (0.04)
Zeaxanthin (cyanobacteria & prochlorophytes)	3.1 (0.06)	4.9 (0.21)	4.9 (0.22)	6.3 (0.15)
"Chlorophyll <i>b</i> " (prasinophytes & prochlorophytes)	13.1 (0.25)	4.8 (0.21)	7.5 (0.33)	6.8 (0.16)

Values are obtained by vertical integrations from 0 to 200 m. Accessory pigment-to-chlorophyll *a* ratios (w:w) are given in parentheses. The RP-HPLC method employed is not capable of separating monovinyl chlorophyll *a* from divinyl chlorophyll *a* nor monovinyl chlorophyll *b* from divinyl chlorophyll *b*.

the nitracline from above and the 1% light level from below (similar to results of *Cullen and Eppley* [1981]; and *Siegel et al.* [1990]). The vertical extent of the chlorophyll maximum envelope and the various pigments is modulated by mesoscale advective features (Figures 13 and 14) as well as deepening or shoaling of the mixed layer and at higher frequencies by internal gravity waves. In particular, the chlorophyll envelope follows the descending isotherms from JD 100 to JD 140 (Figures 7 and

13). The descent of the chlorophyll maximum observed in the heating season is consistent with observations and model results reported by *Strass and Woods* [1988] and *Wolf and Woods* [1988]. They argue that the subsurface chlorophyll maximum results from physical processes and the depletion of nutrients in the upper levels. Nutrient uptake can create a nutricline that slowly descends during the spring with the chlorophyll maximum intensifying and descending with the

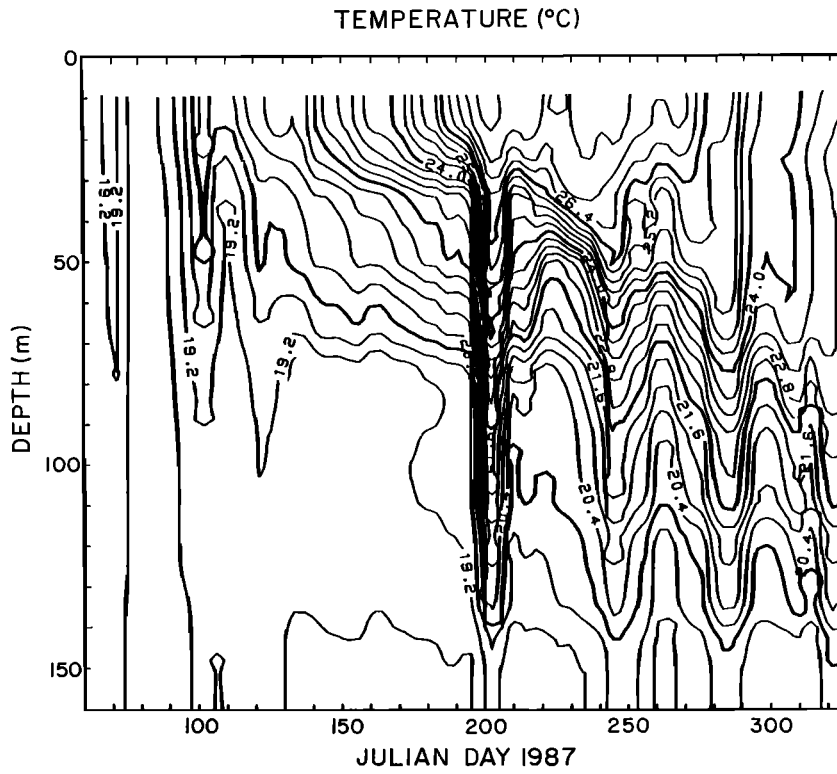


Fig. 13. Time versus depth contours of temperature ( $^{\circ}\text{C}$ ). Note that a 24 h filter was applied before contouring of temperature in the present figure and the variables shown in Figures 14-19.

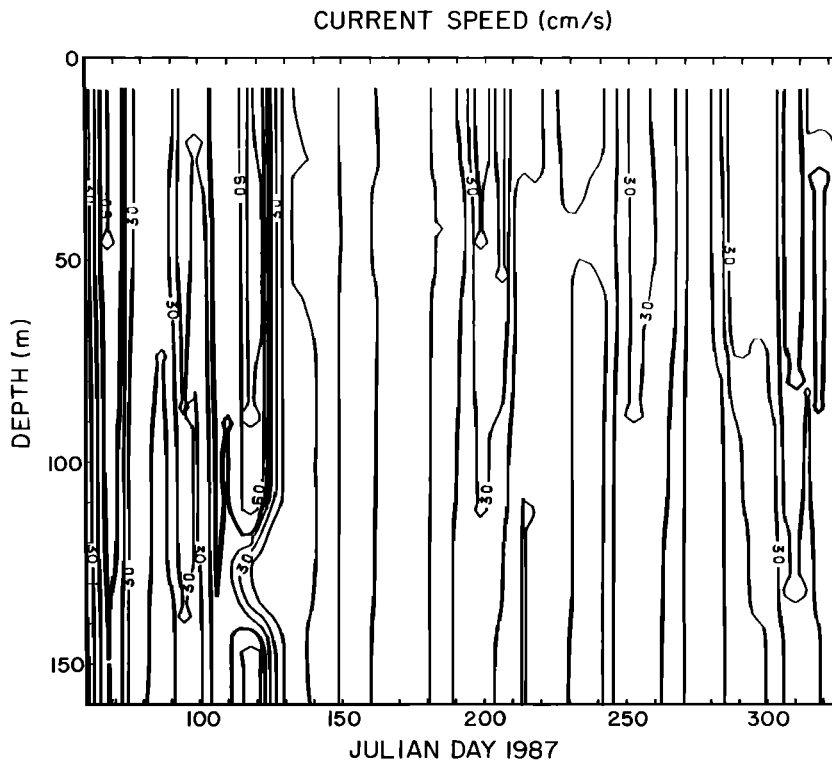


Fig. 14. Time versus depth contours of current speed ( $\text{cm s}^{-1}$ ).

nutricline. It is also likely that biological controls such as sinking (estimated at  $\sim 1 \text{ m d}^{-1}$  using a depth range of 40 to 70 m over a period of JD 100 to JD 130) and grazing are also important [e.g., *Steele and Yentsch, 1960*]. The change in the vertical structure in the pigments is apparent by JD 138-140

(Figure 20) and the depth of the  $0.25 \mu\text{M}$  nitrate level is greater than 60 m.

The effect of an increase of biomass after JD 86 is seen in the PAR/PAR(0), KPAR, beam attenuation coefficient and chlorophyll fluorescence contours (Figures 15, 16, 17, and 18).

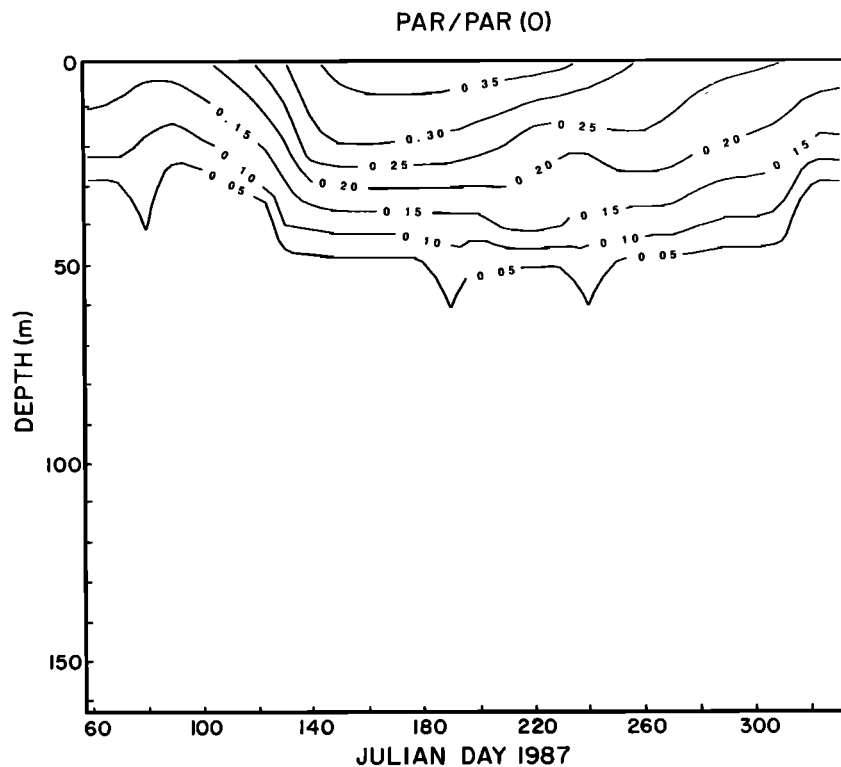


Fig. 15. Time versus depth contours of the ratio of PAR at depth to PAR just below the surface or PAR/PAR(0).

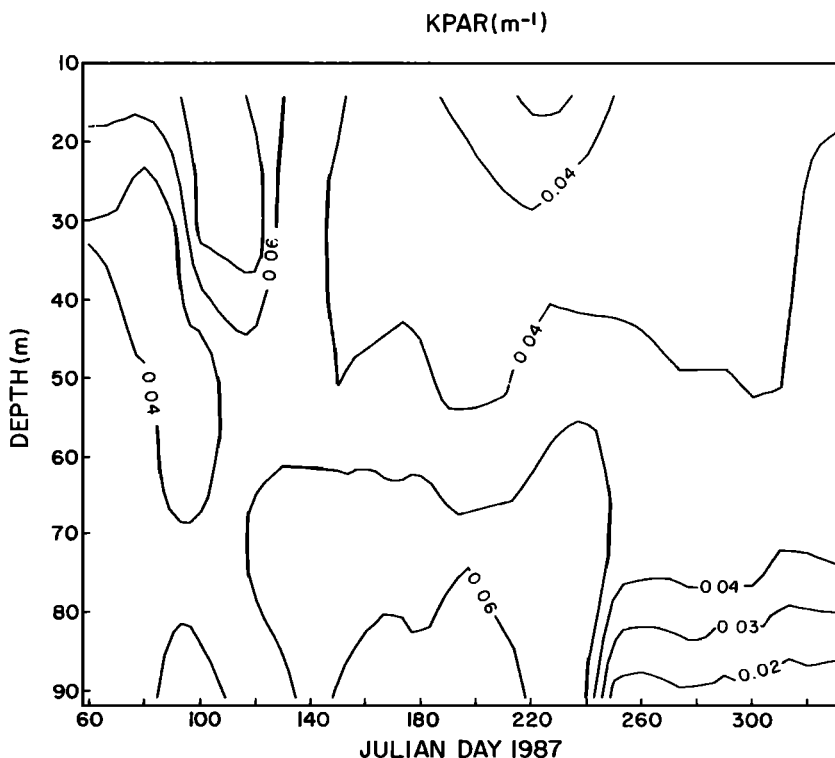


Fig. 16. Time versus depth contours of the diffuse attenuation coefficient of PAR, KPAR in m<sup>-1</sup>.

The BOMS spectral diffuse attenuation coefficient data are consistent with these data as well [Smith et al., 1991].

The signals associated with the dissolved oxygen concentration (Figure 19) reflect variability in temperature, gas exchange and ventilation, and biological productivity and respiration [e.g., Jenkins and Goldman, 1985]. During the first

~20 days of deployment 1, dissolved oxygen is relatively uniform with depth as are temperature and density. The 26.2 isopycnal reaches the surface indicating communication between surface waters and waters to at least 160 m in depth. The significance of this observation is highlighted by Jenkins and Goldman [1985]. It is interesting to note that the evolution

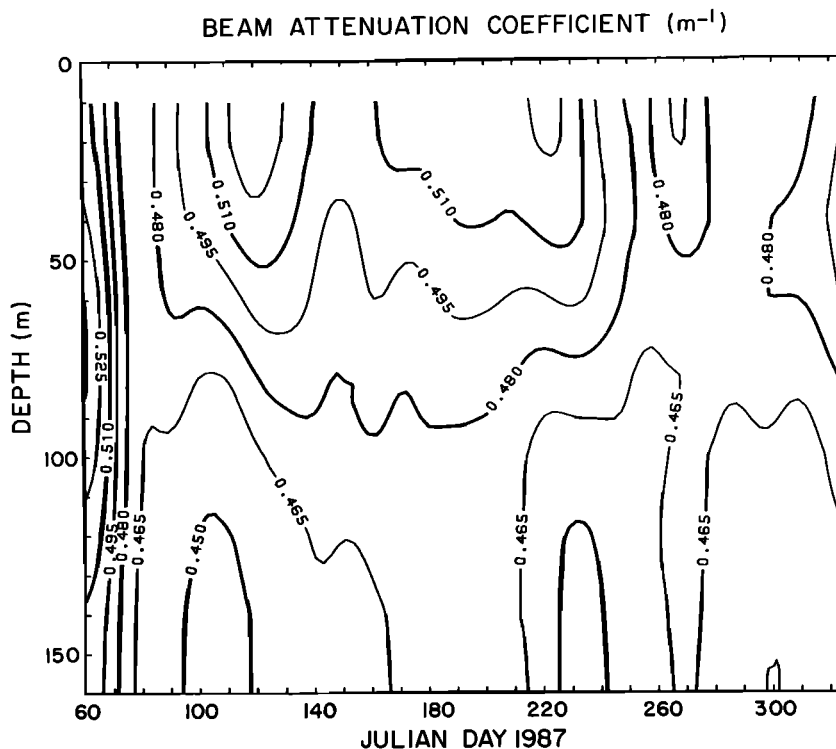


Fig. 17. Time versus depth contours of beam attenuation coefficient ( $m^{-1}$ ).

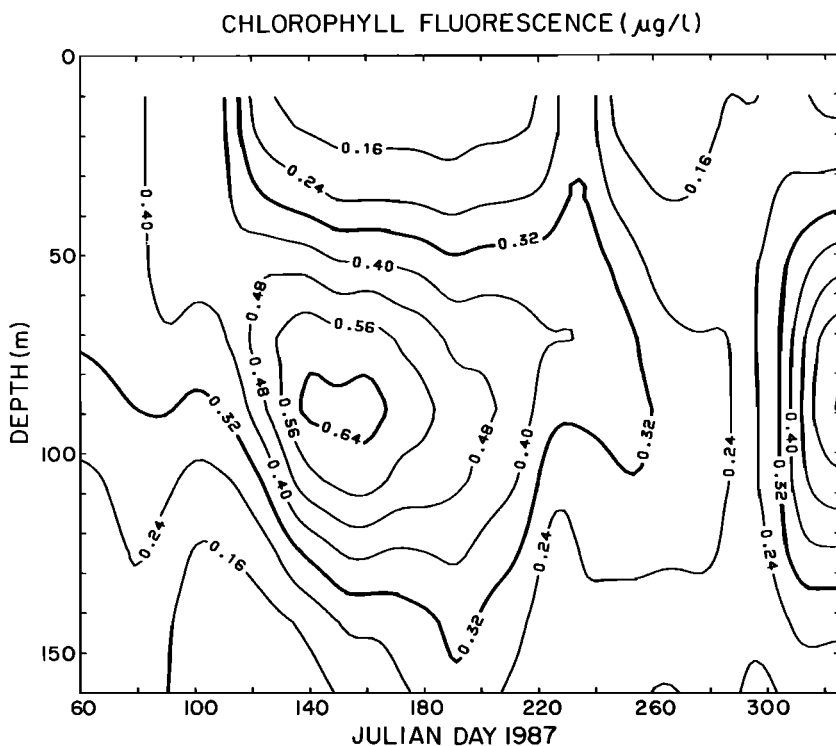


Fig. 18. Time versus depth contours of chlorophyll fluorescence ( $\mu g Chl-a L^{-1}$ ).

of the chlorophyll maximum at depth and the reduction in near surface chlorophyll fluorescence in the summertime appear to be roughly coincident with the formation of a dissolved oxygen maximum of apparent photosynthetic origin (~JD 120) and a summertime decrease in dissolved oxygen. The latter is likely to be the result of warmer temperatures, declining productivity [Marra *et al.*, 1992], and increasing respiratory losses. Our results appear to be generally consistent with the historical data for station S to the south [Jenkins and Goldman, 1985].

*Summary of Deployment 2: Julian Days 136-242, May 16 to August 30, 1987*

The second mooring deployment followed the end of the first by about 6 days. This deployment spans periods 7 through 12 and is generally characterized by summertime seasonal conditions with relatively weak wind forcing, strong solar insolation, warming of a shallow mixed layer, increasing subsurface stratification, and relatively low currents. The

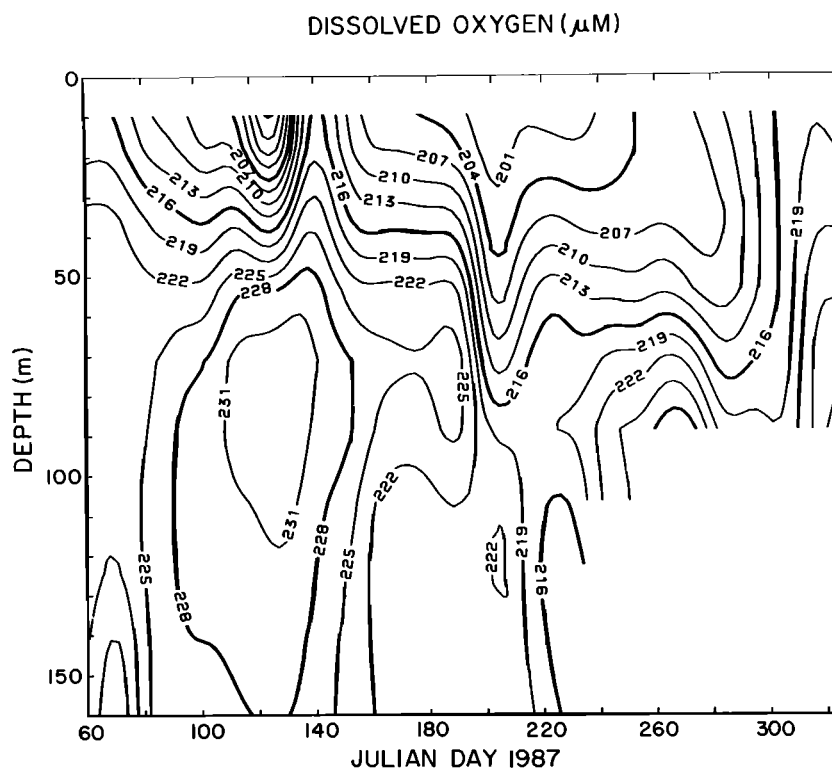


Fig. 19. Time versus depth contours of dissolved oxygen concentration ( $\mu\text{M}$ ).

mixing time scale remains at approximately the same level as observed at the end of deployment 1 (Figure 5) as the wind stress and mixed layer depth are relatively steady during the period. The near surface chlorophyll concentration decreases at the end of deployment 1 to values of less than  $0.2 \mu\text{g L}^{-1}$  and remains near that level throughout the second deployment (Figure 18).

During the late spring to early summer period, reduced mixing time scales and depth-dependent variations in spectral irradiance and nutrients initiate the development of a "chromatically adapted" phytoplankton assemblage which persists through fall (Figure 20). This is accompanied by the broadening of the chlorophyll maximum layer, a decrease in the abundances of cryptophytes and prasinophytes, and an increase in the abundances of photosynthetic dinoflagellates and prochlorophytes (Figure 20 and Table 2). During the summer months, the accessory pigment distributions suggest that the phytoplankton are distributed as three broadly overlapping layers with cyanobacteria (and possibly weakly pigmented prochlorophytes) in the upper water column, prymnesiophytes and chrysophytes at the intermediate depths, and prochlorophytes at the base of the euphotic zone. These algal groups possess unique suites of pigments which allow the efficient utilization of spectral irradiance available for photosynthesis at these depths: (1) blue to green wavelengths: chlorophyll *a* and phycocerythrin of cyanobacteria; (2) blue to blue-green wavelengths: chlorophyll *a*, chlorophyll *c*<sub>2</sub>, chlorophyll *c*<sub>3</sub>, and 19'-acyloxyfucoxanthins of prymnesiophytes and chrysophytes; and (3) blue-green wavelengths: divinyl chlorophyll *b* of prochlorophytes.

The subsurface maximum in chlorophyll concentration, which forms toward the end of the first deployment, persists at a depth of roughly 80-90 m for most of the second deployment (Figure 18) while the depth of the LLL is slightly shallower. The base of the chlorophyll maximum region (Figure 7) tends to follow the trend in the depth of the 1% light level until JD 190 when the most intense mesoscale feature of the experiment is encountered. When solar insolation is low (e.g., periods 2, 3, 11, and 12), this tracking is not as robust. This may be

explained by the argument that as insolation decreases, lower absolute light levels prevail throughout the in situ light field and 1% PAR is no longer a reliable indicator of the lowest light level which will support the phytoplankton population. The depth of the nutricline is unknown except at the beginning and end of the deployment. The depth integrated chlorophyll is relatively great until ~JD 160 when it decreases quite rapidly (see Figure 7b in Marra *et al.* [1992]). The vertical extent of the chlorophyll maximum region begins to decrease from a value of ~60 m to less than ~10 m from JD 180 to JD 220 (Figure 7), again coincident with the occurrence of a major mesoscale event. Bottle cast data indicate that the  $0.25 \mu\text{M}$  nitrate level is below the chlorophyll maximum on JD 235. During JD 195-240 a major ring feature is near the mooring. It is unclear if the upper surface of the chlorophyll maximum envelope was controlled by the nitracline since nitrate concentrations on JD 235 may not be representative of the nitracline depth prior to the advective event. It is interesting to note that following the major mesoscale event (warm outbreak/cold ring sequence of JD 195-240), the chlorophyll envelope descends at a rate of  $\sim 0.7\text{--}0.8 \text{ m d}^{-1}$  from JD 240 to JD 290.

The 1% light level continues to deepen (~60 to ~120 m) until near the end of deployment 2, which is consistent with decreased integrated chlorophyll values. The depth of the LLL is at a depth of ~70 m and continues to track the chlorophyll maximum (Figure 7).

The evolution of the subsurface dissolved oxygen maximum is apparently interrupted by the mesoscale event (~JD 200), whereas the chlorophyll maximum persists. This is likely caused by temperature and water mass effects. The near surface decreases are probably caused by temperature effects. The general evolution of the dissolved oxygen structure is similar to that summarized for station S by Jenkins and Goldman [1985].

*Summary of Deployment 3: Julian Days 243-327, August 31 to November 23, 1987*

The third and final deployment began at the approximate transition between late summer conditions and early fall

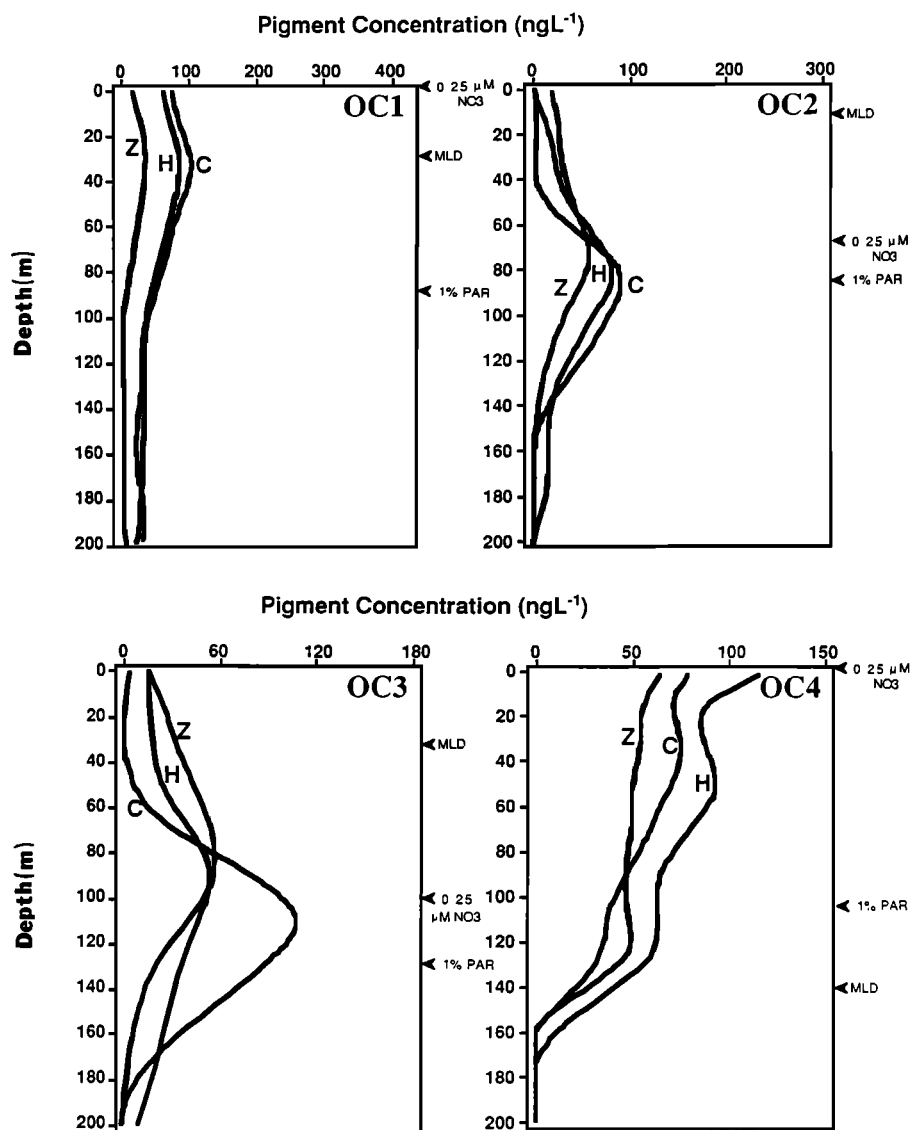


Fig. 20. Vertical profiles of accessory pigment concentrations ( $\text{ng L}^{-1}$ ; Z, zeaxanthin; H, 19'-hexanoyloxyfucoxanthin; and C, "chlorophyll *b*") measured during Biowatt II cruises OC1 (JD 63-67, winter/spring); OC2 (JD 138-140, spring/summer); OC3 (JD 235-237, summer); OC4 (JD 334-335, fall/winter). Profiles are spline-interpolated fits to all accessory pigment data collected during each of the cruises. The RP-HPLC method employed is not capable of separating monovinyl chlorophyll *a* from divinyl chlorophyll *a* nor monovinyl chlorophyll *b* from divinyl chlorophyll *b*.

conditions and ended in late fall, spanning periods 13 through 18. This transition is most easily seen in the deepening of the mixed layer and the cooling of near-surface waters (~JD 270; see Figures 6, 7, and 13). The deepening is associated with increased frequency of more intense atmospheric frontal features and their accompanying higher wind stress and reduced solar insolation due to increased cloudiness and reduced length of day. There is also an increase in the frequency of mesoscale events in the general region and at the mooring site (Figures 2 and 3). This is reflected in increased current speeds and variability (Figure 8). The wind stress increases, while the solar insolation, net heat flux (Figure 5), and PAR (Figure 9) decrease with the seasonal trend. The 1% light level is shallower (Figure 5) during this period than at the end of the previous period and the ratio of PAR/PAR(0) (Figure 15) decreases through the euphotic layer. The LLL depth is variable and on average at about the same depth as during the previous deployment.

During the fall with the breakdown of stratification, the chromatically adapted phytoplankton structure described for deployment 2 is effectively eroded and pigment composition

resembles that observed during the winter/spring period (Figure 20 and Table 2). Isotherms in the chlorophyll maximum envelope are generally deepening (Figures 6 and 13). However, deep warm features (e.g., ~JD 245) interrupting this trend do not appear to modify the deepening chlorophyll maximum envelope (Figure 7). This suggests that the chlorophyll maximum is not descending solely because of water advection. The nutricline (roughly at level of 20.4°C isotherm) is deeper than the chlorophyll envelope at this point and is very near the depth of the 1% PAR level. The low nutrient condition in the upper 100 m may explain why a broader deep chlorophyll maximum region does not form as growth is probably slowed. Further, cells that are not growing optimally probably sink across isopycnal surfaces which may explain the observed deepening of the chlorophyll maximum envelope across isotherms. This process may continue because low light level and nutrient conditions retard growth. Interestingly, the mixed layer depth continues to deepen and may have reached the nutricline, possibly contributing to raised nutrient concentrations (note that the nutricline reaches the surface between the beginning and end of

deployment 3; see discrete values in Figure 7) and thus to higher chlorophyll values after ~JD 300 (Figure 18). The depth integrated (through 200 m) pigment concentrations are very nearly the same on JD 335 as they were on JD 66 (Table 2).

Near surface dissolved oxygen increases after ~JD 220 with the onset of cooling and increasing wind stress. A subsurface maximum in dissolved oxygen, possibly associated with deep cool water, is observed on ~JD 260 between ~80 and 100 m. This maximum is roughly coincident with a beam attenuation coefficient maximum and a deeper lying chlorophyll maximum which occur at the end of the observational period.

The detailed description of the events of deployment 1 are given in Dickey *et al.* [1991] and those of deployments 2 and 3 are presented below.

#### Period 7: Julian Days 136-156, May 16 to June 5, 1987

A major transition in the physical structure takes place between the end of deployment 1 and the beginning of deployment 2 as evidenced by the temperature discontinuity at all depths (decreased values seen in Figure 6) and the transition from the most energetic currents of the experiment to some of the least energetic (Figure 8). There is an apparent advection of cool water past the mooring during the mooring redeployment period. Although the SST map does not resolve this feature, the SSH maps [Chai *et al.*, 1991] do indicate a weak cold core ring structure (Figure 3) which may account for the mooring temperature observation.

The wind forcing is weak (less than 0.2 Pa with some variation due to passage of weak fronts) during this period (Figure 5) and near surface warming continues as does stratification through the upper 80 m (Figures 6 and 7). The local currents are low at all depths, beginning toward the northeast and rotating clockwise (Figure 8). The dominant current signal for this period and much of deployment 2 is at the inertial period (Figure 22).

The near surface (~upper 40 m) chlorophyll concentration remains quite low during this period while the subsurface maximum (values greater than  $\sim 0.8 \mu\text{g l}^{-1}$ ) formed toward the end of period 6 persists (Figure 18). The 1% light level is deeper (~105 m) than during period 6 (Figure 7), while the depth of the LLL increases by ~15 m to a depth of ~80 m.

#### Period 8: Julian Days 156-180, June 5 to June 29, 1987

There is a temporary break (1-2 days) in the trend of increased warming of the upper water column which occurs near the end of period 7 and the beginning of period 8, before temperature continues its seasonal increase. This is apparently caused by a cold mesoscale feature. The SST map of JD 170 suggests the possibility of cold rings to the south and southeast of the mooring (Figure 2). However, SSH maps (JD 171 Figure 3) indicate an elevated SSH feature (inferred clockwise rotation) also to the south of the mooring site. The correct interpretation is not obvious on the basis of these data sets. In any case, the warming and stratification trends resume and the mesoscale advective effect appears to make a relatively small perturbation on the seasonal signal. Such perturbations are not uncommon and are not unexpected considering the current regime of the region; however, these may play significant roles in the exact timing of biologically significant events such as blooms and busts (rapid reduction of phytoplankton concentrations) observed at specific locations.

The local wind forcing is weak and comparable to that of the previous period. The net heat flux is also comparable to the previous period although there are a few days of relatively low heat flux (i.e., JD 169), primarily due to cloudy conditions. A temporary reduction in heating rate (~JD 170) may be related to this; however, changes in the upper ocean temperature time series on the scale of a few days appear to be more affected by

advection. The local currents are quite small as they were during period 7 and generally are directed toward the north. This flow is consistent with a geostrophic flow associated with the apparent warm feature (elevated SSH) to the south of the mooring.

The near surface values of beam attenuation coefficient and chlorophyll fluorescence continue near previous values and the subsurface chlorophyll maximum persists. The 1% light level, though somewhat sporadic, continues its deepening trend while the LLL depth varies by ~20 m with an average depth of ~70 m.

#### Period 9: Julian Days 180-195, June 29 to July 14, 1987

Cool water is encountered at all depths at the mooring site during this period on ~JD 193 (Figure 6), interrupting the seasonal heating trend. The primary mesoscale features described for JD 191 (SSH, Figure 3) are nearly the same as those of JD 181 with two cold rings (north and northeast of the mooring and a warm feature to the southeast). It seems likely that a subtle shift of the currents at the mooring site, probably caused by the movements of the rings and a warm feature, results in the observed subsurface cooling as the winds ( $< 0.1 \text{ Pa}$ ) and the net heat flux is unchanged from the previous period (Figure 5). The currents at the mooring increase significantly during this period (up to  $\sim 50 \text{ cm s}^{-1}$ ) and are directed toward the north-northwest (Figure 8). Despite the physical variability, there are no major changes in the bio-optical properties during the period, suggesting that the advected water masses are not appreciably different biologically.

#### Period 10: Julian Days 195-210, July 14 to July 29, 1987

Following the decrease of temperature at all depths at the end of period 9, the temperature increases rapidly ( $\sim 5^\circ$  at 40-60 m, Figure 6). The currents at the mooring shift from a direction toward the north to a direction toward the southeast between ~JD 195 and ~JD 200 (Figure 8). It appears that cold water is advected toward the north for a couple of days (entered on ~JD 195), then warm water is advected toward the south-southwest with peak temperatures occurring just after JD 200. Then, cold water is apparently again advected past the mooring toward the north until the end of the period. The currents at the mooring are intense (the greatest of deployment 2 peaking at  $\sim 70 \text{ cm s}^{-1}$ ) and toward the southwest when the warmest temperatures are observed (Figure 8). The SST map for JD 201 (Figure 2) suggests that the mooring was near the edge of a cold ring (centered to the north) and a warm outbreak. An AXBT section taken on JD 198 indicates a deep (~700 m) cold core ring centered near  $35^\circ\text{N } 70^\circ\text{W}$  [Dastugue, *et al.*, 1988]. The Geosat map of SSH (JD 211 in Figure 3) suggests a similar interpretation, but with the added indication of northward motion of the warm feature discussed earlier. It is clear that the mesoscale current structure and advective temperature features are complex and strong gradients in temperature and SSH are evident. The temperature variations associated with this event are the greatest of the entire experiment. It is also noteworthy that the greatest near surface temperature for the experiment coincides with this warm advective event with the near surface temperature generally decreasing after this period. The mixed layer depth fluctuates by as much as 15 m due to the event (Figure 7). The wind stress is somewhat greater than during the previous period but still not particularly large ( $< 0.2 \text{ Pa}$ ). The net heat flux is at about the same level as the previous period, but declines significantly in the following period, suggesting that the increase and decrease in heating is caused by a combination of both local and advective forcing.

The chlorophyll maximum region begins to narrow dramatically at this time, and the LLL depth shoals from ~80 to ~55 m. There is also a significant decrease (and then an increase) in dissolved oxygen through the upper 100 m, related to the advective feature.

*Period 11: Julian Days 210 - 220, July 29 to August 8, 1987*

Another warm feature, though less intense than that observed during period 10, is evident during period 11. Both features are observed throughout the upper 160 m with the greatest temperature variations occurring from below the mixed layer down to ~120 m (Figure 6). It should be noted that the temperature and current record at 42 m is absent for this and the following period because of instrumentation malfunction. The wind stress is only slightly greater during this period than during the previous period, however, the net heat flux is considerably less because of reduced solar insolation. The SST map (Figure 2) for JD 219 indicates a possible cold core ring to the northwest of the mooring. The SSH map (Figure 3) shows cold core features, one to the northwest and another to the northeast. A warm feature is southwest of the mooring. Clearly, the site is located in a region of rich mesoscale structure at this time, which probably contributes to the complex temperature time series data. The only major change in the bio-optical properties from the end of the previous period is in the extent of the chlorophyll maximum region, which continues to narrow (Figures 7 and 18). Dissolved oxygen increases after reaching a relative minimum (Figure 19).

*Period 12: Julian Days 220-242, August 8 to 30, 1987*

The temperature map for JD 236 (Figure 2) indicates warm outbreak water encircling a cold core ring to the west-northwest of the mooring site. The Geosat SSH maps are more definitive and show cold core rings in nearly the same position on JD 231 and JD 241 as they were on JD 221 (Figure 3). There is also somewhat weaker evidence of the warm outbreak. The currents decrease in intensity (Figure 8). There is one relatively large wind event (wind stress  $\sim 0.3$  Pa on  $\sim$ JD 225) accompanied by reduced solar radiation and net heat flux (Figure 5). This event may have caused some deepening of the mixed layer and reduced near-surface temperatures, however, these effects appear to be minor. The general trend of subsurface ( $>60$  m) temperature is to increase at the end of the deployment, apparently due to the advection of warm waters. There is little change in the bio-optical properties from the previous period.

*Period 13: Julian Days 242-250, August 30 to September 7, 1987*

There was only a one day break in observations between deployments 2 and 3, however during this interval it appears that the deeper (below mixed layer) temperatures peaked (Figure 6) and more intense currents began (Figure 8). A general decrease in temperature occurred during period 13 (Figure 6). The deepening of the mixed layer (Figure 7) is apparently caused by increased wind stress ( $\sim 0.2$  Pa) and reduced surface net heat flux (Figure 5). It is likely that the advection of cool water is also an important factor for reducing temperature and establishing the exact timing of the deepening just as the advection of warm water increases temperature locally and affects the timing of the onset of the spring transition described earlier.

Along with the transition in the temperature structure between deployments 2 and 3, there is also a transition to considerably increased currents at the site (Figure 8). These currents are directed toward the south-southwest. The sea surface temperature map (Figure 2) indicates the continued presence of a cold core ring encircled by warm outbreak water to the northwest of the mooring site (JD 236 and JD 252 of Figure 2). The Geosat SSH maps (JD 241 and JD 251 of Figure 3) confirm this feature but also indicate a cold core ring nearer and to the north of the site and a diffuse warm feature even nearer to the mooring on JD 241. An XBT map (JD 240) of temperature structure confirms the presence of a cold core ring at  $\sim 35.5^\circ\text{N}$ ,  $70^\circ\text{W}$ , manifest primarily from a depth of 100 m to  $>400$  m [Chai *et al.*, 1991]. The feature is less apparent in temperature at depths less than

$\sim 100$  m. The thermal structure of the upper 100 m is complicated by advection of waters with different origins and the temperature structure is not coherent over depth.

The depth of the chlorophyll maximum increases during this period and continues to increase until  $\sim$ JD 300 (Figure 7). The vertical extent of the chlorophyll maximum region remains quite narrow ( $\sim 10$ - $15$  m). The depth of the 1% light level begins to shoal during the end of deployment 2 and this trend continues during the mooring redeployment phase resulting in a change in the depth of the 1% light level from  $\sim 125$  to  $\sim 105$  m. This could be caused by either increased local production associated with a fall bloom or the advection of a water mass (possibly from a cold core ring) from the north which may have had greater biomass associated with it. On the other hand, the depth of the LLL increases by  $\sim 10$  m from the end of deployment 1 to the end of this period. These opposite trends in the depths of the 1% light level and LLL may be explained by the fact that the LLL depth is shallower than the chlorophyll maximum at this time. Dissolved oxygen continues to increase in the upper layer and a subsurface maximum appears to develop at  $\sim 90$  m.

*Period 14: Julian Days 250-263, September 7 to 20, 1987*

The cold core ring to the north of the mooring as indicated by the Geosat SSH data as early as JD 211 appears in the SST map of JD 259. The presence of warm outbreak waters encircling this ring as well as the cold core ring to the northwest is confirmed by the Geosat SSH data (JD 251 and JD 261 of Figure 3). (Note that there are serious errors in portions of the Geosat derived SSH of JD 261-291; however, we have chosen to include these figures for completeness.) The Geosat data indicate another large, though less intense, warm body of water to the southwest of the mooring. Again, it is evident that the temperature and currents are complex in the region at this time. The meteorological conditions are relatively calm during the period (Figure 5).

The currents at the mooring continue to rotate counterclockwise (Figure 8). The temperature at depths greater than  $\sim 40$  m (below the mixed layer) first increase then decrease (Figure 6). Temperature peaks again a few days later at 42 and 62 m. It is likely that the advection of differing water masses associated with the warm outbreak and cooler Sargasso Sea waters or possibly the cold core rings is taking place. The chlorophyll maximum region continues to deepen and the LLL depth increases by  $\sim 10$  m. The subsurface maximum in dissolved oxygen continues to intensify and the near surface dissolved oxygen is increasing.

*Period 15: Julian Days 263 - 275, September 20 to October 2, 1987*

The SST map indicates two possible cold core rings to the north and northwest of the mooring (JD 268 in Figure 2). These are the same features shown in the SST map of JD 259 and the SSH maps of JD 251 and JD 261. The SSH maps (Figure 3) suggest that on JD 271 the mooring site lies near the two cold core rings generally to the northeast and north-northwest and two more diffuse warm features lying to the southeast and southwest.

The first week of this period is characterized by warming below the mixed layer. The mixed layer gains in heat, then cools for the remainder of the period. Cooling from just below the mixed layer down to about 100 m occurs during the last few days of the period. The greatest rate of cooling is within the upper 25 m. The wind stress remains about the same, but there is reduced solar insolation and net heat flux during a few days of the period which apparently contributes to the near surface cooling. At depths below 100 m, the temperature increases throughout the period. The mixed layer depth remains at about the same depth ( $\sim 25$  m) before deepening rapidly during the next period. Current velocities ( $\sim 20$   $\text{cm s}^{-1}$ ) continue toward the northeast for the first portion of the period but then decrease.

The deepening trend in the chlorophyll maximum continues and the subsurface maximum in dissolved oxygen continues but with reduced intensity (Figure 18). Near surface dissolved oxygen continues to increase (Figure 19). The depth of the LLL varies about an average value of ~75 m.

*Period 16: Julian Days 275-300, October 2 to October 27, 1987*

The dominant feature of this period is a warm outbreak which is relatively intense (second only to that occurring during deployment 1 on ~JD 201) and long in duration (~JD 275 to 295). The expression of this feature is manifest throughout the upper 160 m and clearly interrupts the trend of decreasing near surface temperature and mixed layer deepening (Figures 6 and 7). The SST map for JD 289 (Figure 2) does not show any major mesoscale features in the vicinity of the mooring. However, the Geosat SSH map (Figure 3) for JD 291 indicates the presence of intense warm features, possibly related to those described for the previous period, near the mooring site and centered to the west and the northeast. Unfortunately, the Geosat data are not available for the primary track (running on a diagonal from the southeast to the northwest) on JD 281 when the warm feature is observed at the mooring. The currents at the mooring are low at the beginning and end of the period, but intensify from JD 283 to JD 296. They rotate generally counterclockwise (Figure 8).

There are two passages of significant low atmospheric pressure systems (~JD 274 and 287) and the wind stress is in excess of ~0.4 Pa (Figure 5). The daytime net heat flux is significantly reduced during the first of these events, primarily because of reduced solar radiation resulting from cloudy conditions (Figure 5). The local meteorological forcing does not appear to control the thermal structure even near the surface because of the major warm feature. The overall near surface cooling and mixed layer deepening trends still dominate the period. By the end of this period, the temperature at 14 m has decreased over 3°C since the beginning of the deployment. From JD 270 to JD 300 (Periods 15 and 16), the mixed layer deepens from ~30 m to ~60 m.

The chlorophyll maximum continues to deepen and remains quite narrow while the subsurface maximum in dissolved oxygen appears to be subsiding. There is a continuing trend of increasing near surface chlorophyll fluorescence and dissolved oxygen. The depth of the LLL varies by over 30 m during the period.

*Period 17: Julian Days 300-314, October 27 to November 10, 1987*

Another warm feature, though less intense and shorter in duration, is the primary factor affecting the upper layer during Period 17 (Figure 6). This feature also acts to reduce the cooling trend during this time and convergence and divergence of isotherms associated with the feature leads to modification of the local stratification and mixed layer depth. The mixed layer depth makes excursions from ~60 m to ~85 m and back to ~70 m. The Geosat SSH maps of JD 301 and 311 (Figure 3) indicate that the mooring site lies between warm eddies, one to the northeast and one to the southwest with a cold core ring further to the northeast of the mooring. These features most likely contribute to the observed physical variability. The currents at the mooring site are primarily toward the south-southwest and intensify, peaking around JD 305. The local meteorological forcing is relatively modest ( $\tau < 0.2$  Pa) despite the passage of a major low-pressure system on JD 310 (Figure 4). Currents rotate counterclockwise with velocities ranging from ~30 to 60  $\text{cm s}^{-1}$ .

The most dramatic bio-optical feature is the practical elimination of the chlorophyll maximum (shown as a single line curve in Figure 7). This may be interpreted as being the result of deep mixing. The LLL and 1% PAR depths remain

nearly constant (~70 m and 110 m, respectively), which suggests that the integrated biomass of the upper water column is remaining relatively constant as well. This view is supported by the integrated chlorophyll time series [Marra *et al.*, 1992]. Chlorophyll fluorescence, beam attenuation coefficient, and dissolved oxygen data suggest development of subsurface maxima with chlorophyll showing the most intense signal (Figures 17, 18, and 19).

*Period 18: Julian Days 314 - 327, November 10 to 23, 1987*

The final period of the experiment is characterized by a warm feature, which is similar to that observed during the previous period. The SST map (Figure 2) shows the presence of cold core rings to the northwest and northeast (the cold core ring at ~36°N, 70°W is apparent in the XBT section taken on JD 332) and warm outbreak water to the north encircling the ring to the northwest. These features are also discernible in the SSH maps (Figure 3, JD 311 and JD 321 (note tracking errors in JD 321 map); however, the more dominant features are the warm core eddies, again lying nearer the mooring to the northeast and southwest. The perimeter of the warm eddy to the northeast appears to virtually intersect the mooring site. The currents at the mooring are directed toward the southeast, generally consistent with the RG current map data. The eddy to the northwest is most likely responsible for the temperature increase and decrease at the mooring during this period (from SSH maps for JD 321 and 331). One important difference between this period and the previous period is the resumed near surface cooling (Figure 6). This may possibly be explained by the fact that the most intense winds of the deployment occurred on ~JD 316 along with reduced net heat flux (Figure 5).

An intense chlorophyll maximum region centered at about 80 m is observed (Figure 18). Slightly shallower, less intense subsurface maxima are also apparent in the beam attenuation coefficient and dissolved oxygen (Figures 17 and 19). Elevated values of chlorophyll and diffuse attenuation coefficient (at 441 nm) are also observed at shallower depths from the BOMS data of Smith *et al.* [1991]. The ratio of PAR/PAR(0) decreases significantly during this period as well (Figure 15). It is likely that a water mass with high subsurface biomass advects past the mooring site. It may be speculated that such a water mass may have been associated with a cold core ring or possibly fall bloom waters which advect past the mooring. Unfortunately, our data are not comprehensive enough to test these hypotheses.

#### 4. DISCUSSION

The physical cycle has been observed at the present site previously by Briscoe and Weller [1984] and by others in less detail. The biological (and to a lesser extent the physical) cycle has been observed at a site to the south near Bermuda (32°N, 65°W) by others such as Menzel and Ryther [1960, 1961], Knap *et al.* [1991], and Lohrenz *et al.* [1992]. The basic characteristics of the seasonal cycles are in principle reasonably predictable on coarse time scales. However, the timing of the seasonal transitions and the amplitudes of the physical and bio-optical signals are considerably more difficult to predict. Our time series data indicate that there are a multiplicity of episodic events which act to perturb as well as contribute to the seasonal cycle. The forcing takes the form of local synoptic weather events and advection of water masses related to the instabilities of the Gulf Stream manifest in cold core rings and warm outbreak waters.

The historical meteorological and upper ocean physical data sets indicate the expected seasonal progression also observed in our data sets (e.g., see Briscoe and Weller [1984] for summary). There is some degree of interannual variability, even with

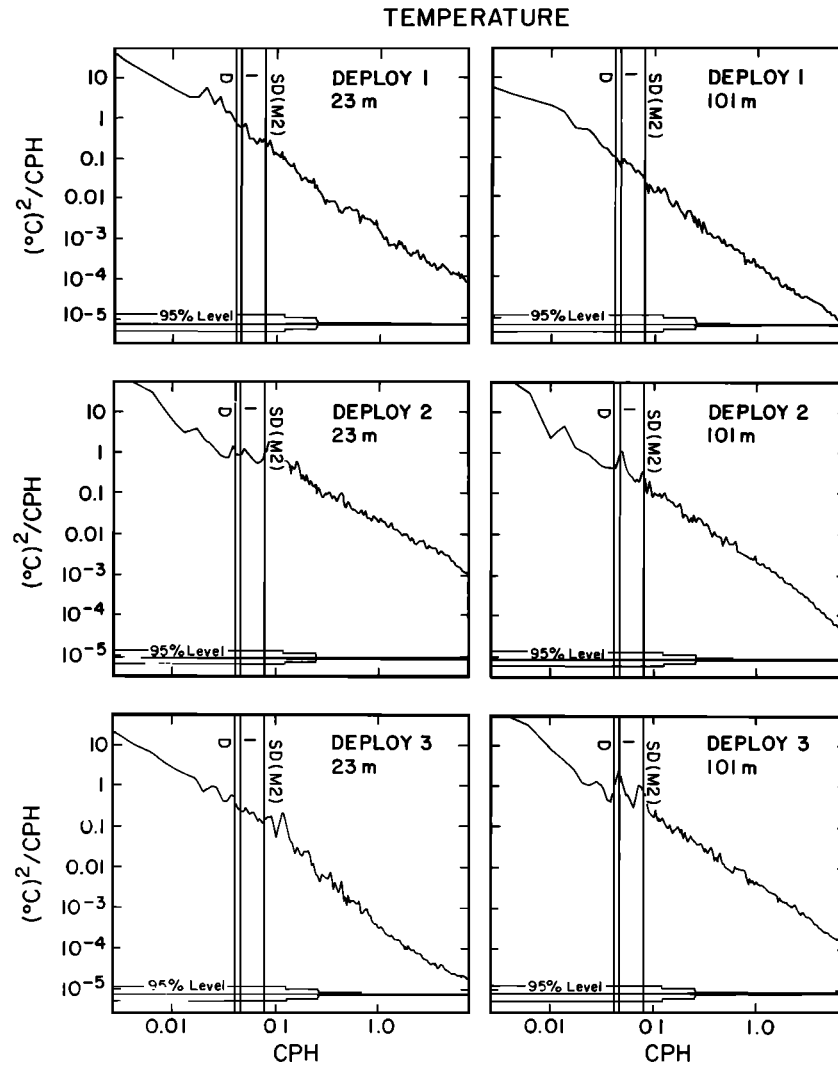


Fig. 21. Spectra of temperature for deployments 1 through 3 for depths of 23 and 101 m. The symbols D, SD, and I indicate diurnal, semidiurnal, and inertial frequencies, respectively. The local inertial period is 21.5 h.

averaging of monthly data over  $1^\circ$  squares surrounding the site. However, the high temporal resolution time series in the upper 200 m of the water column of *Briscoe and Weller* [1984] show considerable variability, obviously associated with advection, especially warm outbreak waters. Their experiment began in May of 1982 and ended in April 1983, enabling the observation of the shoaling of the mixed layer in May (apparently after the actual onset) and the deepening of the mixed layer. It should be noted that our observations did not span the winter months whereas those of *Briscoe and Weller* [1984] miss only a few weeks in April. Their upper layer temperature records indicate that the sea surface temperature began to decrease in August in 1982 and 1983 within a couple of weeks. Interestingly, subsurface warming continued during both years through the end of September while mixed layer deepening and near surface cooling was taking place. It is not clear whether this is associated with the seasonal cycle in some indirect way or is merely a manifestation of subsurface mesoscale features advecting through the site. *Briscoe and Weller* [1984] suggest that the energetic events in the near-inertial field may be related to edge effects of intense mesoscale currents, perhaps being radiated during geostrophic adjustment, rather than solely wind events. Interestingly, *Eriksen et al.* [1982], who did vertical profiling measurements of currents, temperature, and conductivity at a site near Bermuda and to the southeast of the LOTUS site, indicate that sources of shear other than wind

forcing (e.g., baroclinic processes associated with fronts and mesoscale features) appear to be responsible for modification of stratification. The wind forcing is less dynamic at the Bermuda site than at the LOTUS site, so that a direct comparison is not strictly warranted. Our preliminary analysis does not enable us to partition the contributions of these competing processes; however, it is evident by inspection of the data that both local and advective processes are indeed important. Future analysis and modeling of our data set may facilitate the interpretation.

The classical work of *Menzel and Ryther* [1960, 1961] focused on the seasonal cycle of primary production at a site in the Sargasso Sea, about 25 km southeast of Bermuda (station S  $32^\circ\text{N}$ ,  $64^\circ\text{W}$ ). This site has been the subject of observations since 1957 and work there has intensified in the past few years as part of the Joint Global Ocean Flux Study [e.g., *Knap et al.*, 1991; *Lohrenz et al.*, 1992]. The site is in a different oceanic province, both in terms of the physical and bio-optical conditions, than the present site as documented during the Biowatt I study of 1985 [*Siegel et al.*, 1990].

*Menzel and Ryther* [1960, 1961] noted that the factors making the site different from more temperate sites include low nutrient concentrations, clear waters, relatively high solar insolation in winter, shallow mixed layer, and rapid recycling of nutrients. These factors contribute to relatively high wintertime production. In contrast, our site is subject to more intense and frequent atmospheric forcing events, the nutricline and 1% light

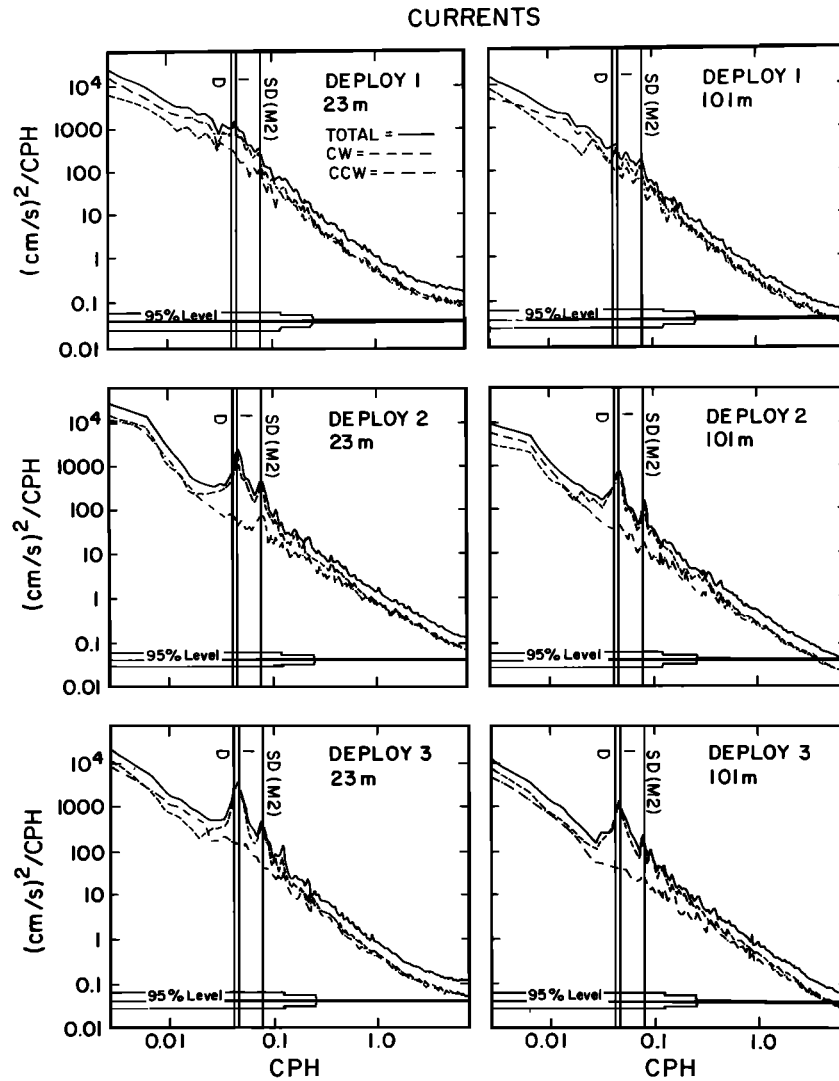


Fig. 22. Rotary spectra of currents at 23 m and 101 m. Symbols are consistent with those of Figure 21. Also, CW and CCW indicate clockwise and counterclockwise components of the rotary spectra.

levels are much shallower, and the phytoplankton biomass and primary productivity are greater. Despite these differences, it is worthwhile to review the seasonal variations at the sites. *Menzel and Ryther* [1960, 1961] measured gross and primary production at station S from November 1957 through April 1959 at bi-weekly intervals. In addition, they collected data including temperature, salinity, nutrients, dissolved oxygen, chlorophyll *a* concentrations, light penetration, and incident radiation. They reported that nutrient (phosphate, nitrate, nitrite, and silicate) concentrations were low in the mixed layer even in the wintertime and showed little seasonal variation. They also indicated that these nutrients were utilized rapidly by phytoplankton. Our data [see *Marra et al.*, 1992] indicate large seasonal variation with greatest near surface values in late winter to early spring and late fall opposed to the summer. With respect to phytoplankton, *Menzel and Ryther* reported the following seasonal sequence: moderately high values of chlorophyll *a* concentrations ( $\sim 0.35\text{--}0.50 \mu\text{g L}^{-1}$ ) with uniform values in depth during the winter and early spring, a spring bloom (peak concentrations of  $\sim 1.0 \mu\text{g L}^{-1}$ ) estimated to be about one month duration in April with the biomass sinking and remaining in the upper euphotic zone for another month, a summer period marked by stratification of the upper water

column and low values of chlorophyll *a* ( $\sim 0.1 \mu\text{g L}^{-1}$  near the surface increasing to  $\sim 0.5 \mu\text{g L}^{-1}$  at 100 m), and a short-lived, minor fall bloom in November and uniform distribution of chlorophyll with depth as stratification subsided and deep mixing developed. Interestingly, the spring blooms of 1958 and 1959 were quite different in both timing (difference of 2.5 months) and duration. The seasonal cycle in chlorophyll *a* observed at the Biowatt II site is generally quite similar to *Menzel and Ryther's* observations. During the Biowatt I experiment in 1985, a bloom occurred in early April [*Marra et al.*, 1990; *Siegel et al.*, 1990; *Bidigare et al.*, 1990]. It is likely that the interannual timing and relative exposure (or lack of exposure) of deep waters ( $18^\circ$  Mode waters) through ventilation plays a substantial role in the timing and intensity of springtime blooms in this general region. Finally, it is interesting to note that values (smoothed) of the phytoplankton crop (based on depth integrated chlorophyll *a*) varied by only about a factor of 2 during our observations (Table 2 and *Marra et al.* [1992]).

Primary production is the focus of our recent paper [*Marra et al.*, 1992]; however, a few summary comments are included here for completeness. *Menzel and Ryther* [1960, 1961] observed high levels of production in the winter and early spring and low levels in late spring through early fall. They noted that

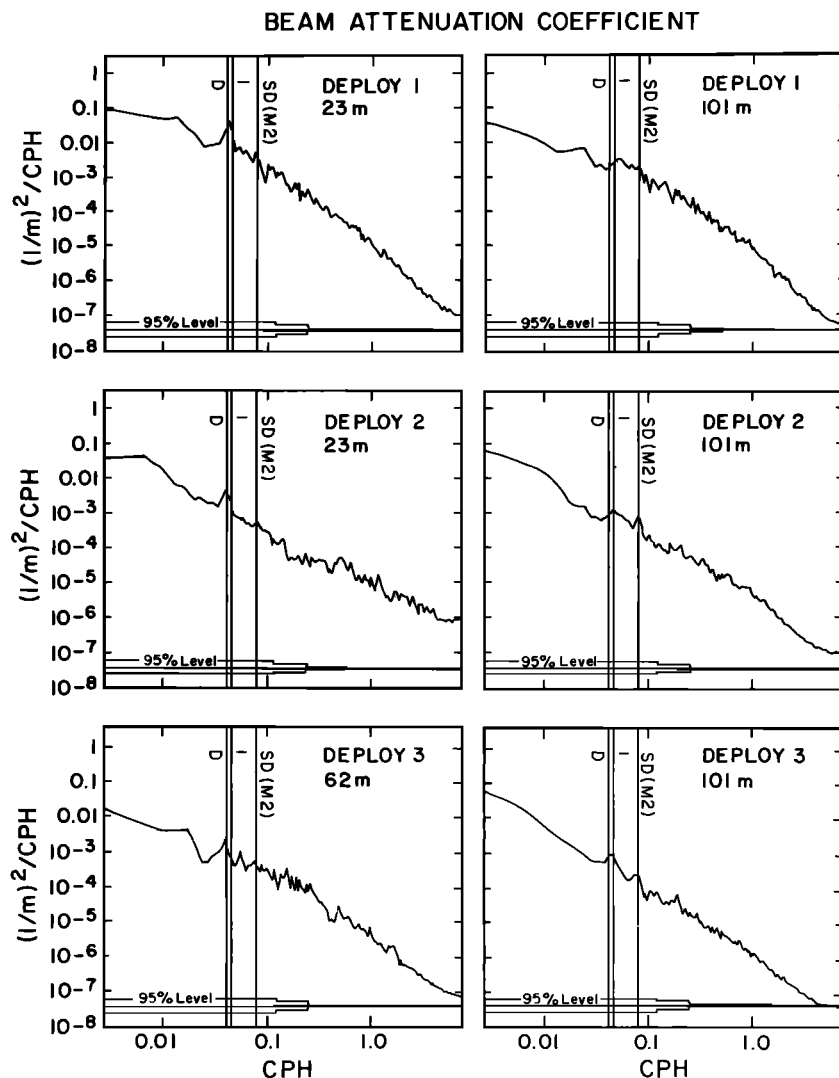


Fig. 23. Spectra of beam attenuation coefficient at 23 m and 101 m (except for deployment 3, where the spectrum for the 62-m depth replaces that of the 23-m depth).

production was closely linked to vertical mixing, with high productivity occurring when the mixed layer reached the upper portion of the permanent thermocline. Gross and net production tracked each other with peak periods occurring in late February and mid-April and appeared to be nutrient rather than light controlled. Despite the relatively coarse temporal measurements, their data suggest considerable variability which is probably associated with both local forcing and occasional mesoscale events. Our production results ( $11.7 \text{ mol C m}^{-2}$  reported in *Marra et al.* [1992]), based on intercomparisons of annual production, are similar to those at station S of *Lohrenz et al.* [1991] ( $8.8\text{--}11.7 \text{ mol C m}^{-2}$ ) but greater than those of *Menzel and Ryther* [1960, 1961] ( $6.8 \text{ mol C m}^{-2}$ ). This is not surprising because of both the geographical and interannual differences. Values of the gross photosynthetic rate (smoothed and depth integrated) varied by only about a factor of 2 during our observations [*Marra et al.*, 1992]. *Altabet* [1989] has estimated the annual new nitrogen flux for a site near Bermuda to be  $0.33 \text{ mol m}^{-2} \text{ yr}^{-1}$ , but suggests that this may be an underestimate as sporadic events may not have been sampled. He also estimated carbon flux using C/N ratios of 9.5 and 7 for sinking and suspended particles respectively, obtaining a value of  $\sim 2.8 \text{ mol C m}^{-2} \text{ yr}^{-1}$ , which is in good agreement with the value estimated by *Jenkins and Goldman* [1985] using oxygen data as described below.

A model of phytoplankton growth and metabolic regulation in combination with a one-dimensional mixed layer model [*Gill and Turner*, 1976] was used by *Kiefer and Kremer* [1981] to examine the seasonal evolution of phytoplankton and nutrients at station S. Their model results reproduce the main features observed at the site. *Menzel and Ryther* [1960] suggested that the deep chlorophyll maximum originated from the sinking of nutrient-impooverished phytoplankton produced in the upper layers whereas *Kiefer and Kremer* [1981] argued that the origin of the subsurface maximum was related to the evolution of the stratification with the chlorophyll remaining within the thermocline until entrained during winter mixing. Both mechanisms may be relevant to the seasonal cycles at station S and our site.

The seasonal cycle of oxygen and primary production using station S data from 1961-1978 was analyzed by *Jenkins and Goldman* [1985] and more recently a model was utilized for a similar purpose by *Musgrave et al.* [1988]. *Jenkins and Goldman* [1985] indicated that the development of a subsurface maximum of oxygen in the euphotic zone at the site must be due to photosynthesis. Our data suggest subsurface structure which is qualitatively consistent with their assertion and with previous data at the station S site [see *Jenkins and Goldman*, 1985; *Musgrave et al.*, 1988]. *Musgrave et al.* [1988] utilized a one-dimensional mixed layer model [based on *Price et al.*, 1986] to simulate the seasonal cycle (composite of years 1961-1970)

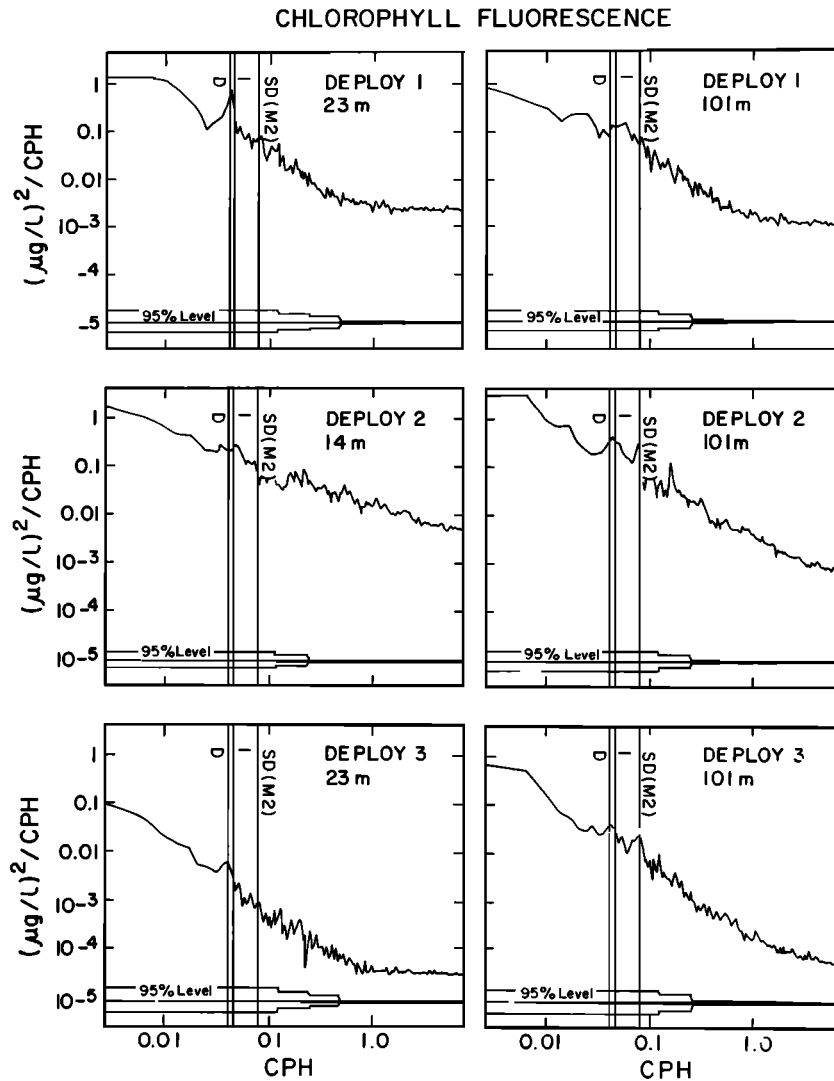


Fig. 24. Spectra of chlorophyll fluorescence at 23 m and 101 m (except for deployment 2, where the spectrum for the 14-m depth replaces that of the 23-m depth).

of temperature and oxygen at station S. The model was also used in a diagnostic mode to estimate new production. They indicate that the major uncertainty in their estimate of production is related to the relationship between gas exchange rate and wind speed and that their annual oxygen production is slightly lower than estimated by *Jenkins and Goldman* [1985] (3.4 versus 5 mol C m<sup>-2</sup>).

As indicated by *Menzel and Ryther* [1960], it is likely that local wind forcing, as well as shears associated with advective features, lead to entrainment of deeper, cooler, and more nutrient rich waters. In particular, short but intense wind events generate inertial currents which can persist for long periods of time and continue to cause high shear at the base of the mixed layer. This shear leads to mixed layer deepening and entrainment of cooler, nutrient rich waters into the upper layer. If the surface waters are nutrient poor prior to the event and light is sufficient, phytoplankton blooms can be facilitated. A likely time for this situation is in the early fall. On the other hand, it is possible that if nutrients and light are sufficiently available to phytoplankton prior to a major wind event, then deepening of the mixed layer and low mean irradiance of phytoplankton over a generation time can lead to a phytoplankton bust. Interestingly, *Klein and Coste* [1984], with work based on numerical simulations, suggest that the time evolution of

nutrient entrainment is not driven by wind stress per se, but rather the wind-surface current interaction (particularly at the inertial scale [e.g., *Dickey and Simpson*, 1983]). They also suggest that at larger scales, the wind forcing is non-uniform in the horizontal and that spatially inhomogeneous distributions of nutrients and phytoplankton would result. The occurrence of local upwelling at frontal boundaries and in cold core rings cannot be discounted either. The antithesis of the wind event forcing is the situation of calm winds and high surface heating which leads to enhanced surface warming and mixed layer and thermocline shoaling. Provided that a sufficient seed population of phytoplankton is present and nutrients are not limiting, a phytoplankton bloom may occur as the phytoplankton exposure time to light is increased as they spend more time in the shallower mixed layer region [e.g., *Sverdrup*, 1953].

The local forcing and response are certainly important for the observed seasonal cycle as manifest in the springtime shoaling of the mixed layer and accompanying phytoplankton blooms and the late fall deepening of the mixed layer. However, it is evident from our data that nonlocal effects must be important for the timing of seasonal transitions of both physical and bio-optical regimes. The maps of SST and SSH indicate that the mooring site is situated in a region of considerable advection

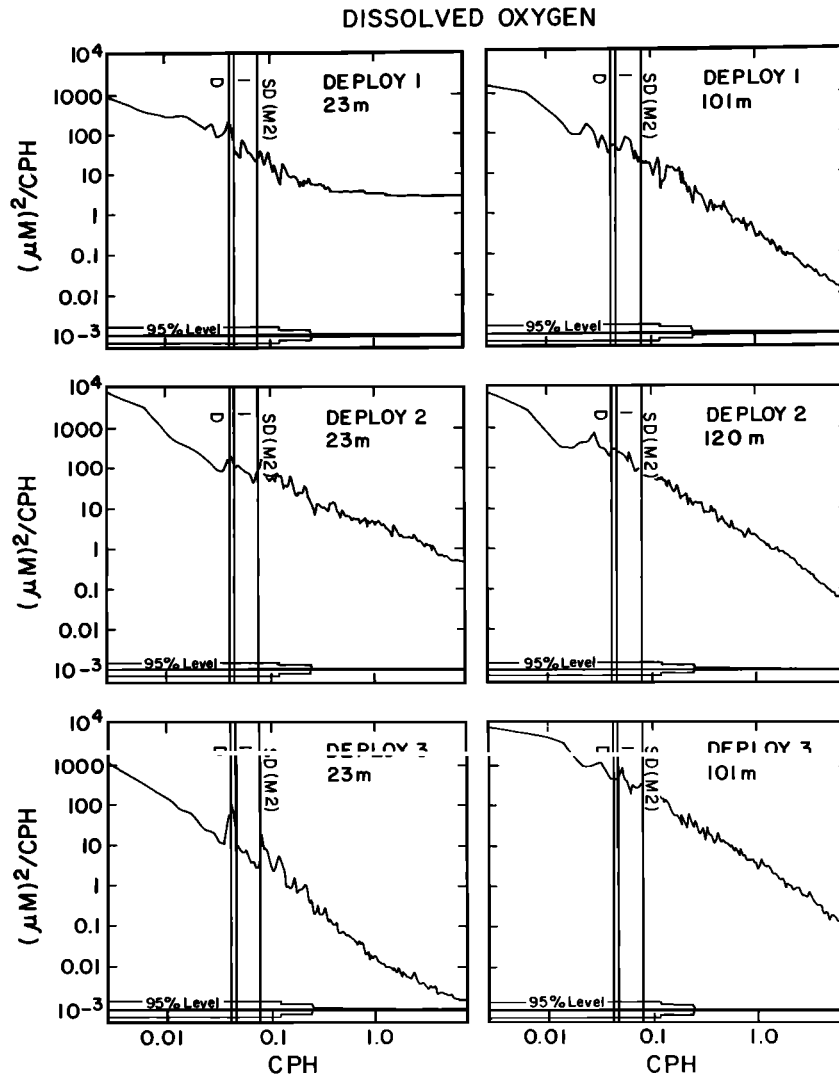


Fig. 25. Spectra of dissolved oxygen concentration at 23 m and 101 m (except for deployment 2, where the spectrum for the 120-m depth replaces that of the 101-m depth).

and water mass variability. Previous analysis of SST and color satellite imagery for the region by *Brown et al.* [1985] indicated spatial variations in phytoplankton biomass and the timing of blooms in different subregions. Our time series of temperature at the mooring site indicate effects of advection manifest in subsurface temperature variations of up to  $-4^{\circ}\text{C}$  over a few days. In the springtime, advection of warm near surface waters can accelerate seasonal stratification of the upper water column. Conversely, the passage of cool waters associated with a cold core ring can accelerate the deepening of the mixed layer in the fall. The observations of high amplitude temperature fluctuations obviously associated with mesoscale advective events are often coincident with high currents. The analysis of satellite color imagery by *Denman and Abbott* [1988] indicates typical mesoscale features of scale 50-100 km with decorrelation times of 7 to 10 days. As an aside, *Bennett and Denman* [1989], using a quasi-geostrophic model of two-dimensional turbulence, concluded that the seasonal cycle of plankton can result in patchiness on the scale of 700 km. Our study reemphasizes the need to include mesoscale and large-scale motions in seasonal models of the seasonal cycle in the geographic region.

The present data set allows us to consider variability in bio-optical properties as well as physical properties. The spectral characteristics of internal gravity waves, generally with

frequencies bound by the local buoyancy frequency and the inertial frequency, have been the subject of many observations. However, most of this work has been limited to physical data, particularly currents and temperature. The autospectra for the present physical and bio-optical variables are subdivided according to deployment for convenience, but as indicated previously, the three deployments roughly coincide with relatively distinct oceanic regimes.

The spectra for wind velocity (not shown) indicate that there is roughly a factor of five more energy at time scales of a day to a few days for the first and third deployment periods than for the second. There is similar spectral energy density at higher frequencies for all three deployments. The autospectra of temperature for 23 and 101 m depths are shown in Figure 21 for each deployment. The autospectra for these depths for the first deployment and for the third deployment at 23 m do not indicate significant spectral peaks at the inertial, semi-diurnal, or diurnal frequencies. This may be related to the high energy levels associated with intense mesoscale and atmospheric forcing and the deeper mixed layers where internal tides would not be supported. Rotary spectra for currents at 23 and 101 m are shown in Figure 22 and indicate greater spectral energy density near the local inertial frequency for deployments 2 and 3. The absence of peaks at the inertial frequency for deployment 1 is probably related to the mesoscale variability giving

broadly distributed energy at lower frequencies. The clockwise rotation component is greater for deployments 2 and 3 than its counterclockwise counterpart as expected for inertial motion in the northern hemisphere. Rotary spectra for the second and third deployments of the Biowatt II experiment give results for the inertial peak which are of the same order of magnitude as those obtained by *Briscoe and Weller* [1984]. The first deployment current spectra indicate the presence of more energy in the low-frequency mesoscale bands than is observed in the two later deployments. These same characteristics for the spring to early summer time frame were reported for the current power spectra determined with current profilers by *Eriksen* [1988], who conducted two 3.5-month time series studies (spring/summer and fall/winter) as part of LOTUS.

In interpreting the spectra of the bio-optical properties, it is important to keep in mind the several processes (summarized earlier) which may affect these variables. One of the most evident aspects of the bio-optical (beam attenuation coefficient, chlorophyll fluorescence, and dissolved oxygen) autospectra is the diurnal peak for depths within the euphotic layer (Figures 23-25). There is also some indication of a peak at the semi-diurnal frequency for these variables during the second and third deployments below the mixed layer (e.g., 101 m). In addition, a semi-diurnal peak is apparent for dissolved oxygen at 23 m as well as for the latter two deployments. Short time scale variability of the bio-optical properties (induced by clouds) has been considered in a separate paper by *Stramska and Dickey* [1992a] and diurnal variability has been considered by *Hamilton et al.* [1990] (also see reports of other work done in Sargasso Sea by *Prezelin and Glover* [1991]).

The temporal variability of the several quantities in the internal gravity wave frequency domain is highly dependent on the vertical displacement of their distributions. A spectral power law is determined from the slope of the log of the variance/unit frequency of the parameter of interest with respect to the log of the frequency. Power law relations such as the ones given by *Garrett and Munk* [1972] for currents and temperature indicate that the spectral energy density,  $S$ , is generally inversely proportional to the square of the frequency or  $S \sim \omega^{-n}$  with  $n = 2$  in a frequency domain somewhat greater than the inertial frequency (here  $f \sim 0.05$  cph) and less than the buoyancy frequency (here  $N \sim 2.7$  cph). The power law formalism is useful in that it characterizes the rate of transfer of internal wave energy between scales, generally from large scales (lower frequencies) to smaller scales (higher frequencies). Our spectra for currents, temperature, and beam transmission are in good agreement with this  $n = 2$  power law. However, a power of  $n \sim 1.6$  is obtained for chlorophyll fluorescence and dissolved oxygen. It is possible that beam attenuation generally acts as a passive scalar tracer for the time scales relevant to internal gravity waves. Chlorophyll fluorescence measurements are perhaps more complicated because of short time scale variability related to processes such as photoadaptation and photoinhibition (near the surface). Also, for deployment 1 when biological activity was great, near surface spectral rolloff for dissolved oxygen and fluorescence is at time scales less than 2-5 h. This may be related to photoprocesses or possibly instrument response.

## 5. SUMMARY

The present study clearly indicates that important processes associated with and contributing to the seasonal cycle occur on short time and space scales and that aliasing (e.g., insufficient sampling) is a major concern. While the seasonal patterns are discernable from coarse temporal sampling [e.g., *Menzel and Ryther*, 1960, 1961], the understanding and modeling of the seasonal physical and bio-optical processes requires both high temporal and high spatial resolution data collected over broad

regions of the ocean for several years [e.g., *Jenkins and Goldman*, 1985; *Brown et al.*, 1985; *Smith et al.*, 1987; *Altabet*, 1989; *McClain et al.*, 1990; *Dickey*, 1991]. Clearly, a combination of sampling methods is necessary [e.g., *Dickey*, 1991]. Within the next few years, it is likely that it will be possible to obtain data collected virtually concurrently from moorings such as the one described here along with remotely sensed surface data from satellites for temperature, ocean color (e.g., pigment concentrations and diffuse attenuation coefficients), and surface elevation for geostrophic currents. The present study benefitted greatly from both the currents obtained from the mooring and the Geosat SSH (and geostrophic current) maps. However, the lack of ocean color maps and only limited SST maps from satellites restricted analysis and limited our interpretation and potential for modeling. Even with new satellites, moored measurements will continue to be important as they are unaffected by cloud cover and can in principle be used for long-term, uninterrupted, and high-frequency sampling of depths inaccessible with satellite sensors. Optimally, the combined data sets obtained from moorings, ships, drifters, and satellites will be synthesized using appropriate data assimilation models to produce three-dimensional maps of the key physical and bio-optical variables for the estimation and prediction of primary productivity, penetrative component of solar radiation, and carbon fluxes of the upper ocean [e.g., *Dickey*, 1991].

*Acknowledgments.* This research was sponsored by the Office of Naval Research as part of the Biowatt program (contracts N00014-87-K0084 (T.D.) and N00014-86-K0204 (J.M.)). We wish to acknowledge the technical assistance provided by Derek Manov, Miguel Maccio, John Scott, Ivars Bitte, and Larry Sullivan. Thanks are due Bob Weller for providing meteorological data and Victor Zlotnicki for his suggestions concerning the Geosat data set analysis. We acknowledge and appreciate the several comments and suggestions given by John Cullen and anonymous reviewers which greatly improved this paper.

## REFERENCES

- Ackleson, S. G., J. J. Cullen, J. Brown, and M. P. Lesser, Some changes in optical properties of marine phytoplankton in response to high light intensity, *Proc. SPIE Int. Soc. Opt. Eng.*, **X**, 238-249, 1990.
- Altabet, M. A., Particulate new nitrogen fluxes in the Sargasso Sea, *J. Geophys. Res.*, **94**, 12,771-12,779, 1989.
- Baker, E. T., and J. W. Lavelle, The effect of particle size on the light attenuation coefficient of natural suspensions, *J. Geophys. Res.*, **89**, 8197-8202, 1984.
- Bartz, R., J. R. V. Zaneveld, and H. Pak, A transmissometer for profiling and moored observations in water, *Proc. SPIE Int. Soc. Opt. Eng.*, **V**, 102-108, 1978.
- Bartz, R., R. Spinrad, and J. C. Kitchen, A low power, high resolution, in situ fluorometer for profiling and moored applications in water, *Proc. SPIE Int. Soc. Opt. Eng.*, **IX**, 157-170, 1988.
- Bennett, A. F., and K. L. Denman, Large-scale patchiness due to an annual plankton cycle, *J. Geophys. Res.*, **94**, 823-829, 1989.
- Bidigare, R. R., and M. E. Ondrusek, *Biowatt II Data Report*, Department of Oceanography, Texas A&M University, College Station, 49pp., 1988.
- Bidigare, R. R., O. Schofield, and B. B. Prezelin, Influence of zeaxanthin on quantum yield of photosynthesis of *Synechococcus* clone WH7803 (DC2), *Mar. Ecol. Prog. Ser.*, **56**, 177-188, 1989.
- Bidigare, R. R., J. Marra, T. D. Dickey, R. Iturriaga, H. Pak, and R. C. Smith, Evidence for phytoplankton succession and chromatic adaptation in the Sargasso Sea during springtime 1985, *Mar. Ecol. Prog. Ser.*, **60**, 113-122, 1990.
- Bishop, J. K. B., The correction and suspended matter calibration of Sea Tech transmissometer data, *Deep Sea Res.*, **33**, 121-134, 1986.
- Booth, C. R., The design and evaluation of a measurement system for photosynthetically active quantum scalar irradiance, *Limnol. Oceanogr.*, **19**, 326-335, 1976.
- Brewer, P. G., K. W. Bruland, R. W. Eppley, and J. J. McCarthy, The Global Ocean Flux Study (GOFS): Status of the U.S. GOFS Program, *Eos Trans. AGU*, **67**, 827-832, 835-837, 1986.

- Briscoe, M. G., and R. A. Weller, Preliminary results from the Long-Term Upper-Ocean Study (LOTUS), *Dyn. Atmos. Oceans*, **8**, 243-265, 1984.
- Brown, O. B., R. H. Evans, J. W. Brown, H. R. Gordon, R. C. Smith, and K. S. Baker, Phytoplankton blooming off the U.S. east coast: a satellite description, *Science*, **229**, 163-167, 1985.
- Bunker, A. F., Computations of surface energy flux and annual air-sea interaction cycles of the North Atlantic Ocean, *Mon. Weather Rev.*, **104**, 1122-1140, 1976.
- Chai, Z., T. Dickey, J. Vazquez, and J. Wiggert, Observations of mesoscale features in the Sargasso Sea in 1987 using satellite, ship-based, and mooring measurements, *Tech. Rep. OPG-91-01*, 160 pp., Univ. of Southern California, Los Angeles, 1991.
- Cheney, R. E., B. C. Douglas, R. W. Agreen, L. Miller, D. L. Miller, and N. S. Doyle, Geosat altimeter geophysical data record, *NOAA Tech. Memo. NOS NGS-46*, Natl. Oceanic and Atmos. Admin., Rockville, Md., July 1987.
- Cornillon, P., D. Evans, and W. Large, Warm outbreaks of the Gulf Stream into the Sargasso Sea, *J. Geophys. Res.*, **91**, 6583-6596, 1986.
- Cullen, J. J., and R. W. Eppley, Chlorophyll maximum layers of the Southern California Bight and possible mechanisms of their formation and maintenance, *Oceanol. Acta.*, **4**, 23-32, 1981.
- Cullen, J. J., and M. R. Lewis, The kinetics of algal photoadaptation in the context of vertical mixing, *J. Plankton Res.*, **10**, 1039-1069, 1988.
- Dastgue, J. M., Z. R. Hallock, W. J. Teague, and J. L. Mitchell, REX AXBT data in the northwest Atlantic, July 1987, *NORDA Tech. Note 391*, 10 pp., Stennis Space Center, Miss., Nov. 1988.
- Dean, J. P., and R. C. Beardsley, A Vector-Averaging Wind Recorder (VAWR) system for surface meteorological measurements in CODE (Coastal Ocean Dynamics Experiment), *Tech. Rep. WHOI Ref. 88-20*, 74 pp., Woods Hole Oceanogr. Inst., Woods Hole, Mass., 1988.
- Denman, K. L., and M. R. Abbott, Time evolution of surface chlorophyll patterns from cross-spectrum analysis of satellite color images, *J. Geophys. Res.*, **93**, 6789-6798, 1988.
- Denman, K. L., and A. E. Gargett, Time and space scales of vertical mixing and advection of phytoplankton in the upper ocean, *Limnol. Oceanogr.*, **28**, 801-815, 1983.
- Denman, K. L., and A. E. Gargett, Multiple thermoclines are barriers to vertical exchange in the subarctic Pacific during SUPER, May 1984, *J. Mar. Res.*, **46**, 77-103, 1988.
- Deser, C., R. A. Weller, and M. G. Briscoe, Long-Term Upper-Ocean Study (LOTUS) at 34°N, 70°W: Meteorological sensors, data, and heat fluxes for May - October 1982 (LOTUS-3 and LOTUS-4), *Tech. Rep. WHOI-83-22*, 68 pp., Woods Hole Oceanogr. Inst., Woods Hole, Mass., 1983.
- Dickey, T., The emergence of concurrent high resolution physical and bio-optical measurements in the upper ocean and their applications, *Rev. Geophys.*, **29**, 383-413, 1991.
- Dickey, T. D., and J. J. Simpson, The sensitivity of upper ocean structure to time varying wind direction, *Geophys. Res. Lett.*, **10**, 133-136, 1983.
- Dickey, T. D., E. O. Hartwig, and J. Marra, The Biowatt bio-optical and physical moored measurement program, *Eos Trans. AGU*, **67**, 650, 1986.
- Dickey, T., T. Granata, M. Hamilton, J. Wiggert, D. Manov, D. Siegel, Z. Chai, M. Stramska, and J. Scott, Final report on the multi-variable moored system (MVMS) and meteorological data sets collected during the Biowatt II experiment in the Sargasso Sea in 1987, *Tech. Rep. OPG-90-01*, 215 pp., Univ. of Southern Calif., Los Angeles, 1990a.
- Dickey, T., T. Granata, M. Hamilton, J. Wiggert, J. Marra, C. Langdon, and D. A. Siegel, Time series observations of bio-optical properties in the upper layer of the Sargasso Sea, *Proc. SPIE Int. Soc. Opt. Eng.*, **X**, 202-214, 1990b.
- Dickey, T., J. Marra, T. Granata, C. Langdon, M. Hamilton, J. Wiggert, D. Siegel, and A. Bratkovich, Concurrent high-resolution bio-optical and physical time series observations in the Sargasso Sea during the spring of 1987, *J. Geophys. Res.*, **96**, 8643-8663, 1991.
- Eriksen, C. C., Variability in the upper-ocean internal wave field at a Sargasso Sea site, *J. Phys. Oceanogr.*, **18**, 1495-1513, 1988.
- Eriksen, C. C., J. M. Dahlen, and J. T. Shillingford, An upper ocean moored current and density profiler applied to winter conditions near Bermuda, *J. Geophys. Res.*, **87**, 7879-7902, 1982.
- Falkowski, P. G., Light-shade adaptation in marine phytoplankton, in *Primary Productivity of the Sea*, edited by P. G. Falkowski, pp. 99-119, Plenum, New York, 1980.
- Falkowski, P. G., Physiological responses of phytoplankton to natural light regimes, *J. Plankton Res.*, **6**, 295-307, 1984.
- Falkowski, P. G., and D. A. Kiefer, Chlorophyll-*a* fluorescence in phytoplankton: relationship to photosynthesis and biomass, *J. Plankton Res.*, **7**, 715-731, 1985.
- Garrett, C., and W. Munk, Space-time scales of internal waves, *Geophys. Fluid Dyn.*, **2**, 225-264, 1972.
- Gill, A. E., and J. S. Turner, A comparison of seasonal thermocline models with observations, *Deep Sea Res.*, **23**, 391-401, 1976.
- Gonella, J., A rotary-component method for analyzing meteorological and oceanographic vector time series, *Deep Sea Res.*, **19**, 833-846, 1972.
- Hamilton, M., T. Granata, T. Dickey, J. Wiggert, D. Siegel, J. Marra, and C. Langdon, Diurnal variations of bio-optical properties in the Sargasso Sea, *Proc. SPIE Int. Soc. Opt. Eng.*, **X**, 214-224, 1990.
- Jenkins, W. J., and J. C. Goldman, Seasonal oxygen cycling and primary production in the Sargasso Sea, *J. Mar. Res.*, **43**, 465-491, 1985.
- Kiefer, D. A., and J. N. Kremer, Origins of vertical patterns of phytoplankton and nutrients in the temperate, open ocean: a stratigraphic hypothesis, *Deep Sea Res.*, **28A**, 1087-1105, 1981.
- Kiefer, D. A., W. S. Chamberlin, and C. R. Booth, Natural fluorescence of chlorophyll-*a*: relationship to photosynthesis and chlorophyll concentration in the western South Pacific gyre, *Limnol. Oceanogr.*, **34**, 868-881, 1989.
- Klein, P., and B. Coste, Effects of wind-stress variability on nutrient transport into the mixed layer, *Deep Sea Res.*, **31**, 27-31, 1984.
- Knap, A. H., A. F. Michaels, R. L. Dow, R. J. Johnson, K. Gundersen, G. A. Knauer, S. E. Lohrenz, V. A. Asper, M. Tuel, H. Ducklow, H. Quinby, and P. Brewer, October 1988-September 1989, 110 pp., Bermuda Biological Station for Research, Inc., St. Georges, Bermuda, 1991.
- Kondo, J., Air-sea bulk transfer coefficients in diabatic conditions, *Boundary Layer Meteorol.*, **9**, 91-112, 1975.
- Langdon, C., Dissolved oxygen monitoring system using a pulsed electrode: Design, performance, and evaluation, *Deep Sea Res.*, **31**, 1357-1367, 1984.
- Langdon, C., On the causes of interspecific differences in the growth-irradiance relationship for phytoplankton, Part I, A comparative study of the growth-irradiance relationship of three marine phytoplankton species: *Skeletonema costatum*, *Olisthodiscus luteus* and *Gonyaulax tamarensis*, *J. Plankton Res.*, **9**, 459-482, 1987.
- Langdon, C., On the causes of interspecific differences in the growth-irradiance relationship for phytoplankton, Part I, A general review, Part II, *J. Plankton Res.*, **10**, 1291-1312, 1988.
- Le Traon, P. Y., Time scales of mesoscale variability and their relationship with space scales in the North Atlantic, *J. Mar. Res.*, **49**, 467-492, 1991.
- Liu, W. T., T. V. Blanc, T. Liu, K. Katsaros, and J. Businger, Bulk atmospheric flux computational iteration program in FORTRAN and BASIC, *Mem. Rep. 5291*, Nav. Res. Lab., Washington, D. C., 1984.
- Lohrenz, S. E., G. A. Knauer, V. L. Asper, M. Tuel, A. H. Knap, and A. F. Michaels, Seasonal and interannual variability in primary production and particle flux in the northwestern Sargasso Sea: U.S. JGOFS Bermuda Atlantic Time Series, *Deep Sea Res.*, in press, 1992.
- Marra, J., R., R. Bidigare, and T. D. Dickey, Nutrients and mixing, chlorophyll and phytoplankton growth, *Deep Sea Res.*, **37**, 127-143, 1990.
- Marra, J., T. Dickey, W. S. Chamberlin, C. Ho, T. Granata, D. A. Kiefer, C. Langdon, R. Smith, K. Baker, R. Bidigare, and M. Hamilton, The measurement of seasonal primary production from moored optical sensors in the Sargasso Sea, *J. Geophys. Res.*, **97**, 7399-7412, 1992.
- McClain, C. R., W. E. Esaias, G. C. Feldman, J. Elrod, D. Endres, J. Firestone, M. Darzi, R. Evans, and J. Brown, Physical and biological processes in the North Atlantic during the first GARP Global Experiment, *J. Geophys. Res.*, **95**, 18,027-18,048, 1990.
- Mellor, G. L., and T. Yamada, Development of a turbulence closure model for geophysical fluid problems, *Rev. Geophys. Space Phys.*, **20**, 851-875, 1982.
- Menzel, D. W., and J. H. Ryther, The annual cycle of primary production in the Sargasso Sea off Bermuda, *Deep Sea Res.*, **6**, 351-367, 1960.
- Menzel, D. W., and J. H. Ryther, Annual variations in primary production of the Sargasso Sea off Bermuda, *Deep Sea Res.*, **7**, 282-288, 1961.
- Mitchell, J. L., W. J. Teague, and Z. R. Hallock, REX AXBT data in the

- northwest Atlantic, *NORDA Tech. Rep. 196*, 86 pp., Naval Ocean Res. and Dev. Activity, Stennis Space Center, Miss., 1985.
- Mitchell, J. L., W. J. Teague, Z. R. Hallock, and J. M. Dastugue, REX data in the northwest Atlantic, April 1987, 212 pp., *NORDA Tech. Note 390*, Naval Ocean Res. and Dev. Activity, Stennis Space Center, Miss., 1988.
- Mitchell, J., J. Dastugue, W. Teague, and Z. Hallock, The estimation of geoid profiles in the northwest Atlantic from simultaneous satellite altimetry and airborne expendable bathythermograph sections, *J. Geophys. Res.*, **95**, 17,965-17,977, 1990.
- Morel, A., and A. Bricaud, Inherent optical properties of algal cells including picoplankton: theoretical and experimental results, *Can. Bull. Fish. Aquat. Sci.*, **214**, 521-559, 1986.
- Musgrave, D. L., J. Chou, and W. J. Jenkins, Application of a model of upper ocean physics for studying seasonal cycles, *J. Geophys. Res.*, **93**, 15,679-15,700, 1988.
- Nelson, D. M., and W. O. Smith, Sverdrup revisited: critical depths, maximum chlorophyll levels, and control of Southern Ocean productivity by the irradiance-mixing regime, *Limnol. Oceanogr.*, **36**, 1650-1661, 1991.
- Olson, R., S. W. Chisholm, E. R. Zettler, and E. V. Armbrust, Pigments, size, and distributions of *Synechococcus* in the North Atlantic and Pacific Oceans, *Limnol. Oceanogr.*, **35**, 45-58, 1990.
- Picaut, J., A. J. Busalacchi, M. J. McPhaden, and B. Camusat, Validation of the geostrophic method for estimating zonal currents at the equator from Geosat altimeter data, *J. Geophys. Res.*, **95**, 3015-3024, 1990.
- Porter, D. L., S. M. Glenn, E. B. Dobson, and A. R. Robinson, GEOSAT: a U.S. Navy spaceborne altimeter, *Oceanus*, **33**, 50-57, 1990.
- Prezelin, B. B., and H. E. Glover, Variability in time/space estimates of phytoplankton, biomass and productivity in the Sargasso Sea, *J. Plankton Res.*, **13**, 45-67, 1991.
- Prezelin, B. B., M. M. Tilzer, O. Schonfield, and C. Haese, The control of the production process of phytoplankton by the physical structure of the aquatic environment with special reference to its optical properties, *Aquat. Sci.*, **53**, 136-186, 1991.
- Price, J. F., R. A. Weller, and R. Pinkel, Diurnal cycling: observations and models of the upper ocean response to diurnal heating, cooling, and wind mixing, *J. Geophys. Res.*, **91**, 8411-8427, 1986.
- Siegel, D. A., and T. D. Dickey, On the parameterization of irradiance for ocean photoprocesses, *J. Geophys. Res.*, **92**, 14,648-14,662, 1987.
- Siegel, D. A., R. Iturriaga, R. R. Bidigare, R. C. Smith, H. Pak, T. D. Dickey, J. Marra, and K. S. Baker, Meridional variations of the springtime phytoplankton community in the Sargasso Sea, *J. Mar. Res.*, **48**, 379-412, 1990.
- Smith, R. C., O. B. Brown, F. E. Hoge, K. S. Baker, R. H. Evans, R. N. Swift, and W. E. Esaias, Multiplatform sampling (ship, aircraft, and satellite) of a Gulf Stream warm core ring, *Appl. Opt.*, **26**, 2068-2081, 1987.
- Smith, R. C., K. J. Waters, and K. S. Baker, Optical variability and pigment biomass in the Sargasso Sea as determined using deep-sea optical mooring data, *J. Geophys. Res.*, **96**, 8665-8686, 1991.
- Spinrad, R. W., H. Glover, B. W. Ward, L. A. Codispoti, and G. Kullenberg, Suspended particle and bacterial maxima in Peruvian coastal waters during a cold water anomaly, *Deep Sea Res.*, **36**, 715-733, 1989.
- Steele, J. H., and C. S. Yentsch, The vertical distribution of chlorophyll, *J. Mar. Biol. Assoc. U.K.*, **39**, 217-226, 1960.
- Stramka, M., and T. D. Dickey, Short-term variations of the bio-optical properties of the ocean in response to cloud-induced irradiance fluctuations, *J. Geophys. Res.*, **97**, 5713-5721, 1992a.
- Stramka, M., and T. D. Dickey, Variability of bio-optical properties of the upper ocean associated with diel cycles in phytoplankton population, *J. Geophys. Res.*, **97**, 1992b.
- Strass, V., and J. D. Woods, Horizontal and seasonal variation of density and chlorophyll profiles between the Azores and Greenland, in *Toward a Theory on Biological-Physical Interactions in the World Ocean*, edited by B. J. Rothschild, pp. 113-136, Kluwer Academic Publishers, The Hague, Netherlands, 1988.
- Sverdrup, H. U., On the conditions for vernal blooming of phytoplankton, *J. Cons. Perm. Int. Explor. Mer.*, **18**, 287-295, 1953.
- Swift, E., J. Van Keuren, H. P. Batchelder, C. R. Booth, and C. P. Li, Moored instrument to measure stimulated and natural oceanic bioluminescence, *Ocean Opt.*, **9**, 75-86, 1988.
- Vazquez, J., Observations on the long-period variability of the Gulf Stream downstream of Cape Hatteras, Ph.D. dissertation, *Univ. of So. Calif.*, Los Angeles, 1991.
- Vazquez, J., V. Zlotnicki, and L.-L. Fu, Sea level variability in the Gulf Stream between Cape Hatteras and 50°W: a Geosat study, *J. Geophys. Res.*, **95**, 17,957-17,964, 1990.
- Weller, R., and R. E. Davis, A vector measuring current meter, *Deep Sea Res.*, **27**, 565-582, 1980.
- Weller, R. A., D. L. Rudnick, R. E. Payne, J. P. Dean, N. J. Pennington, and R. P. Trask, Measuring near-surface meteorology over the ocean from an array of surface moorings in the Subtropical Convergence Zone, *J. Atmos. Oceanic Technol.*, **7**, 85-103, 1990.
- Willebrand, J., R. H. Kaese, D. Stammer, H.-H. Hinrichsen, and W. Krauss, Verification of Geosat sea surface topography in the Gulf Stream extension with surface drifting buoys and hydrographic measurements, *J. Geophys. Res.*, **95**, 3007-3014, 1990.
- Wolf, K. U., and J. D. Woods, Lagrangian simulation of primary production in the physical environment: deep chlorophyll maximum and nutricline, in *Toward a Theory on Biological-Physical Interactions in the World Ocean*, edited by B. J. Rothschild (ed.), 51-70, Kluwer Academic Publishers, 1988.
- Zlotnicki, V., A. Hayashi, and L.-L. Fu, The JPL-OCEANS-8902 version of the Geosat altimetry data, *JPL Tech. Rep.*, Jet Propulsion Lab., Pasadena, Calif., June 1, 1989.
- R. Bidigare, Department of Oceanography, University of Hawaii, 1000 Pope Road, Honolulu, HI 96882.
- Z. Chai-Jochner, T. Dickey, T. Granata, M. Stramka, and J. Wiggert, Ocean Physics Group, Department of Geological Sciences, University of Southern California, Los Angeles, CA 90089-0740.
- M. Hamilton and J. Vazquez, Jet Propulsion Laboratory, 4800 Oak Grove Drive, Pasadena, CA 91109.
- C. Langdon and J. Marra, Lamont-Doherty Geological Observatory of Columbia University, Palisades, NY 10964.
- D. Siegel, Center for Remote Sensing and Environmental Optics, University of California, Santa Barbara, CA 93106.

(Received February 17, 1992;  
revised July 25, 1992;  
accepted August 5, 1992.)